

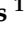







## Article

# A 5-(2-Pyridyl)tetrazolate Complex of Molybdenum(VI), Its Structure, and Transformation to a Molybdenum Oxide-Based Hybrid Heterogeneous Catalyst for the Epoxidation of Olefins

Martinique S. Nunes<sup>1</sup>, Diana M. Gomes<sup>1</sup> , Ana C. Gomes<sup>1</sup> , Patrícia Neves<sup>1</sup> , Ricardo F. Mendes<sup>1</sup> ,  
Filipe A. Almeida Paz<sup>1</sup> , André D. Lopes<sup>2,3</sup>, Anabela A. Valente<sup>1,\*</sup> , Isabel S. Gonçalves<sup>1</sup>   
and Martyn Pillinger<sup>1,\*</sup> 

- <sup>1</sup> Department of Chemistry, Campus Universitário de Santiago, CICECO—Aveiro Institute of Materials, University of Aveiro, 3810-193 Aveiro, Portugal; nunes.m@ua.pt (M.S.N.); dianamgomes@ua.pt (D.M.G.); agomes1@ua.pt (A.C.G.); pneves@ua.pt (P.N.); rfmenes@ua.pt (R.F.M.); filipe.paz@ua.pt (F.A.A.P.); igoncalves@ua.pt (I.S.G.)
- <sup>2</sup> Center of Marine Sciences, CCMAR, Gambelas Campus, University of Algarve, UAlg, 8005-139 Faro, Portugal; adlopes@ualg.pt
- <sup>3</sup> Department of Chemistry and Pharmacy, Faculty of Sciences and Technology, FCT, Gambelas Campus, University of Algarve, UAlg, 8005-139 Faro, Portugal
- \* Correspondence: atav@ua.pt (A.A.V.); mpillinger@ua.pt (M.P.)



**Citation:** Nunes, M.S.; Gomes, D.M.; Gomes, A.C.; Neves, P.; Mendes, R.F.; Paz, F.A.A.; Lopes, A.D.; Valente, A.A.; Gonçalves, I.S.; Pillinger, M. A 5-(2-Pyridyl)tetrazolate Complex of Molybdenum(VI), Its Structure, and Transformation to a Molybdenum Oxide-Based Hybrid Heterogeneous Catalyst for the Epoxidation of Olefins. *Catalysts* **2021**, *11*, 1407. <https://doi.org/10.3390/catal11111407>

Academic Editors: Kotohiro Nomura, Raffaella Mancuso, Takeshi Ohkuma, Fabio Ragaini, Martin Kotorá, Alfonso Grassi, Carl Redshaw, Armando Pombeiro, Ken-ichi Fujita, Carmine Capacchione, Kei Manabe and Victorio Cadierno

Received: 5 November 2021

Accepted: 17 November 2021

Published: 20 November 2021

**Publisher's Note:** MDPI stays neutral with regard to jurisdictional claims in published maps and institutional affiliations.



**Copyright:** © 2021 by the authors. Licensee MDPI, Basel, Switzerland. This article is an open access article distributed under the terms and conditions of the Creative Commons Attribution (CC BY) license (<https://creativecommons.org/licenses/by/4.0/>).

**Abstract:** There is a considerable practical interest in discovering new ways to obtain organomolybdenum heterogeneous catalysts for olefin epoxidation that are easier to recover and reuse and display enhanced productivity. In this study, the complex salt  $(\text{H}_2\text{pytz})[\text{MoO}_2\text{Cl}_2(\text{pytz})]$  (**1**) (Hpytz = 5-(2-pyridyl)tetrazole) has been prepared, structurally characterized, and employed as a precursor for the hydrolysis-based synthesis of a microcrystalline molybdenum oxide/organic hybrid material formulated as  $[\text{MoO}_3(\text{Hpytz})]$  (**2**). In addition to single-crystal X-ray diffraction (for **1**), compounds **1** and **2** were characterized by FT-IR and Raman spectroscopies, solid-state  $^{13}\text{C}\{^1\text{H}\}$  cross-polarization (CP) magic-angle spinning (MAS) NMR, and scanning electron microscopy (SEM). Compounds **1** and **2** were evaluated as olefin epoxidation catalysts using the model reaction of *cis*-cyclooctene (Cy8) with *tert*-butyl hydroperoxide (TBHP), at 70 °C, which gave 100% epoxide selectivity up to 100% conversion. While **1** behaved as a homogeneous catalyst, hybrid **2** behaved as a heterogeneous catalyst and could be recovered for recycling without showing structural degradation or loss of catalytic performance over consecutive reaction cycles. The substrate scope was broadened to monoterpene *DL*-limonene (Lim) and biobased unsaturated fatty acid methyl esters, methyl oleate (MeOle), and methyl linoleate (MeLin), which gave predominantly epoxide products.

**Keywords:** molybdenum; molybdenum oxide; organic-inorganic hybrid material; tetrazole; 5-(2-pyridyl)tetrazole; hydrogen bonds; epoxidation; bio-olefins

## 1. Introduction

Tetrazoles are synthetic five-membered heterocycles containing four nitrogen atoms in the ring [1–4]. They have the highest nitrogen content among the stable unsubstituted heterocyclic systems. Although the tetrazole group has been known for well over a century, since the synthesis of 2-phenyl-2H-tetrazole-5-carbonitrile by the Swedish chemist J.A. Bladin in 1885 [5], systematic studies of tetrazole derivatives only began during the second half of the 20th century. Tetrazoles play important roles in coordination chemistry as ligands with multiple coordination modes [2], in medicinal chemistry as surrogates of the carboxylic acid function [3,4,6–9], and in materials science for the synthesis of nitrogen-rich high-energy-density materials [10]. The most interesting compounds containing tetrazole moieties are 5-substituted tetrazoles, particularly those that contain six-membered nitrogen heterocyclic substituents [3,4,11–15]. Among the numerous multidentate ligands, the rigid

ligand 5-(2-pyridyl)-1*H*-tetrazole (Hpytz) is especially attractive. Hpytz can coordinate to metals in a bidentate fashion through the pyridyl nitrogen and N1 of the tetrazole ring. Under complexation, Hpytz is often deprotonated to the tetrazolate anion (pytz<sup>−</sup>), which opens up a plethora of possible chelating and bridging coordination modes [16–18] that can lead to molecular complexes, multinuclear clusters, and extended one-dimensional (1D), 2D, and 3D structures.

The coordination chemistry of (H)pytz has been mostly studied with respect to d-block elements in groups 7–12 of the periodic table (Mn, Fe, Co, Ni, Cu, Zn, Ag, Cd) [16–33]. To the best of our knowledge, a cyanide complex of Mo<sup>IV</sup>, with the formula (PPh<sub>4</sub>)<sub>2</sub>[Mo(CN)<sub>3</sub>O(pytz)]<sub>2</sub>·H<sub>2</sub>O, is the only compound reported to date that comprises pytz<sup>−</sup> coordinated to Mo centers in a bidentate fashion [34]. Similarly, the 3D Mo/O/Mn<sup>II</sup>/tetrazole compound [Mn(pytz)Mo<sub>2</sub>O<sub>7</sub>] appears to be the only example where a tetrazole moiety bridges adjacent Mo centers (in this case, the tetrazolate anion adopts a bridging  $\mu_{1,2,3,4}$  coordination mode to simultaneously connect two Mo atoms and two Mn atoms, with the pyridyl nitrogen left uncoordinated) [20]. In other related organic-inorganic hybrids based on isopolymolybdate anions, [Mo<sub>x</sub>O<sub>y</sub>]<sup>*n*−</sup> [35–37], or Keggin-type anions, [XMo<sub>12</sub>O<sub>40</sub>]<sup>*n*−</sup> (X = P, Ge) [16,17,38,39], the pytz<sup>−</sup> ligand coordinates exclusively with the secondary metal (Ag or Cu) to generate binuclear or polymeric (1D/2D) metal-organic subunits that interlink with the polyoxoanions. The rarity of Mo-(H)pytz binding contrasts quite sharply with the numerous compounds known containing Mo atoms coordinated to the structurally analogous pyrazole derivative, i.e., 2-[3(5)-pyrazolyl]pyridine (pypz). In complexes such as *cis*-[Mo(CO)<sub>4</sub>(pypz)] [40], [MoO(O<sub>2</sub>)<sub>2</sub>(pypz)] [41], [MoO<sub>2</sub>Cl<sub>2</sub>(pypz)] [42], [Mo<sub>2</sub>O<sub>4</sub>( $\mu_2$ -O)Cl<sub>2</sub>(pypz)<sub>2</sub>] [42], and [Mo<sub>4</sub>O<sub>12</sub>(pypz)<sub>4</sub>] [40,43], the metal centers are *N,N*-chelated in a bidentate fashion by the pypz ligand. Hydrolysis of [MoO<sub>2</sub>Cl<sub>2</sub>(pypz)] gave the hybrid material [Mo<sub>3</sub>O<sub>9</sub>(pypz)]<sub>*n*</sub>, in which one of the structural components consists of 1D chains of corner-sharing {MoO<sub>4</sub>N<sub>2</sub>} octahedra [41]. Good results have been achieved using these Mo/pypz compounds as catalysts or catalyst precursors for the epoxidation of olefins with alkyl hydroperoxides as oxidants [40–42].

In the present work, bidentate coordination of the pytz<sup>−</sup> anion to a Mo<sup>VI</sup> center has been crystallographically confirmed in the newly prepared complex (H<sub>2</sub>pytz)[MoO<sub>2</sub>Cl<sub>2</sub>(pytz)] (**1**). A molybdenum oxide-based hybrid organic-inorganic compound, formulated as [MoO<sub>3</sub>(Hpytz)] (**2**), has been prepared by the hydrothermal hydrolysis of **1**. The molybdenum-catalyzed epoxidation of *cis*-cyclooctene (Cy8) was selected as a benchmark reaction to evaluate the catalytic properties of **1** and **2**, and material **2** was further tested in the epoxidation of biobased olefins.

## 2. Results and Discussion

### 2.1. Catalyst Synthesis and Characterization

The reaction, performed in solution, between the complex [MoO<sub>2</sub>Cl<sub>2</sub>(THF)<sub>2</sub>] [42] and two equivalents of the ligand Hpytz led to the exclusive formation of the compound (H<sub>2</sub>pytz)[MoO<sub>2</sub>Cl<sub>2</sub>(pytz)] (**1**) in good yield. The phase purity of the bulk sample was confirmed by the good match between its powder X-ray diffraction (PXRD) pattern and that simulated from the single-crystal structure (Figure 1). When a 1:1 metal-to-ligand stoichiometry was used in the synthesis (with the intention of obtaining the complex [MoO<sub>2</sub>Cl<sub>2</sub>(Hpytz)]), compound **1** (Supplementary Materials) was still the sole product of the reaction, with a decreased yield of 22%. Compound **1** can be handled in air for short periods and is soluble in polar solvents such as acetonitrile, acetone, and THF.

A single-crystal X-ray diffraction study of compound **1** confirmed that it is a salt, ultimately formulated as (H<sub>2</sub>pytz)[MoO<sub>2</sub>Cl<sub>2</sub>(pytz)]. The compound crystallizes in the non-centrosymmetric space group *Ia*, with the asymmetric unit being composed of a molybdenum(VI) anionic complex that co-crystallizes with a H<sub>2</sub>pytz<sup>+</sup> cation, as depicted in Figure 2. The Mo<sup>VI</sup> center has a distorted {MoCl<sub>2</sub>O<sub>2</sub>N<sub>2</sub>} octahedral coordination environment, being hexacoordinated to two chloride anions, two oxido groups, and a pytz<sup>−</sup> anionic residue. The pytz<sup>−</sup> anionic residue is bound to the metal center through *N,N*-chelation (Figure 2).

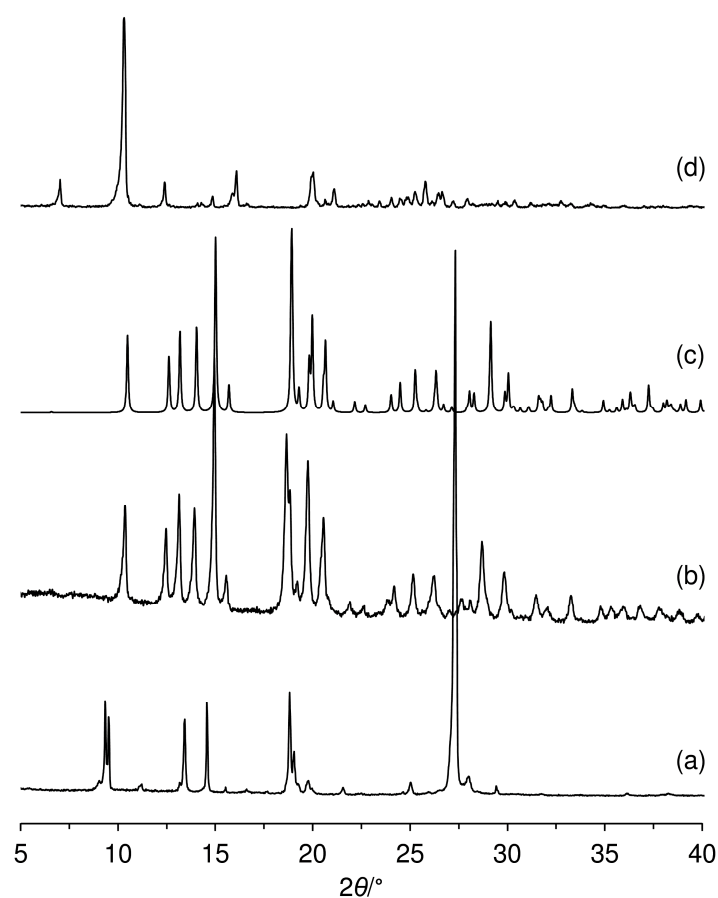


**Figure 1.** Experimental (a,b,d) and computed (c) powder X-ray diffraction (PXRD) patterns of (a) 5-(2-pyridyl)-1*H*-tetrazole (Hpytz), (b,c) (H<sub>2</sub>pytz)[MoO<sub>2</sub>Cl<sub>2</sub>(pytz)] (**1**), and (d) [MoO<sub>3</sub>(Hpytz)] (**2**). The program Mercury (copyright CCDC, ver. 3.9) [44] was used to generate the computed pattern from the crystal structure for **1**.

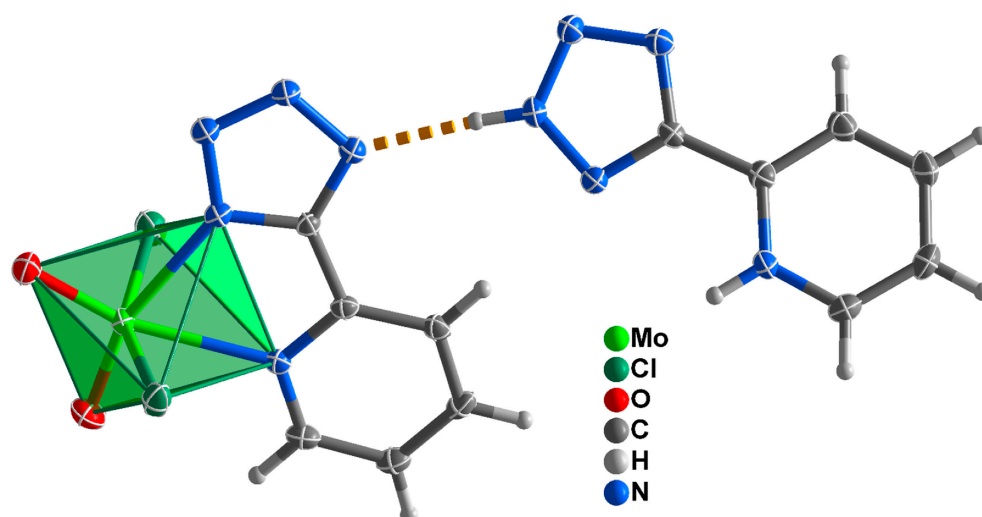


**Figure 2.** Schematic representation of the asymmetric unit of compound **1**, emphasizing the intermolecular hydrogen bond between the anionic metal complex and the neighboring H<sub>2</sub>pytz<sup>+</sup> cation (dashed orange line). Atomic labelling has been omitted for clarity. Selected bond lengths (Å) and angles (°) for the Mo<sup>VI</sup> coordination environment: Mo1—O1 1.692(2), Mo1—O2 1.691(2), Mo1—N1 2.377(2), Mo1—N2 2.286(2), Mo1—Cl1 2.3729(9), Mo1—Cl2 2.3685(9), O2—Mo1—O1 106.09(11), N2—Mo1—N1 69.38(10), Cl2—Mo1—Cl1 157.22(3).

The uncoordinated  $\text{H}_2\text{pytz}^+$  cationic residue interacts with the anionic complex through hydrogen bonding interactions (Figures 2 and 3). In fact, this organic residue is rich in both donor and acceptor groups, which promotes a rather complex network of supramolecular interactions mediating the crystal packing, which also involves the inorganic core of the anionic complexes. For example, Figure 3a depicts the connection of one anionic complex to two neighboring cations by way of several  $\text{N-H}\cdots\text{N}$  interactions with the  $d_{\text{N}\cdots\text{N}}$  distances found in the 2.766(3)–3.306(4) Å range and the corresponding  $\langle\text{NHN}\rangle$  interaction angles in the 133–173° range. These connections are further strengthened by the existence of  $\text{C-H}\cdots(\text{N,O})$  hydrogen bonding interactions, as shown in Figure 3a ( $d_{\text{C}\cdots(\text{N,O})}$  found in the 3.307(4)–3.319(4) Å range with the corresponding  $\langle\text{CH(N,O)}\rangle$  interaction angles in the range 138–147°). Moreover, connections between adjacent anionic complexes are further ensured by  $\pi$ - $\pi$  interactions between adjacent pyridine rings (Figure 3b,  $d_{\pi\cdots\pi} = 3.913(2)$  Å).

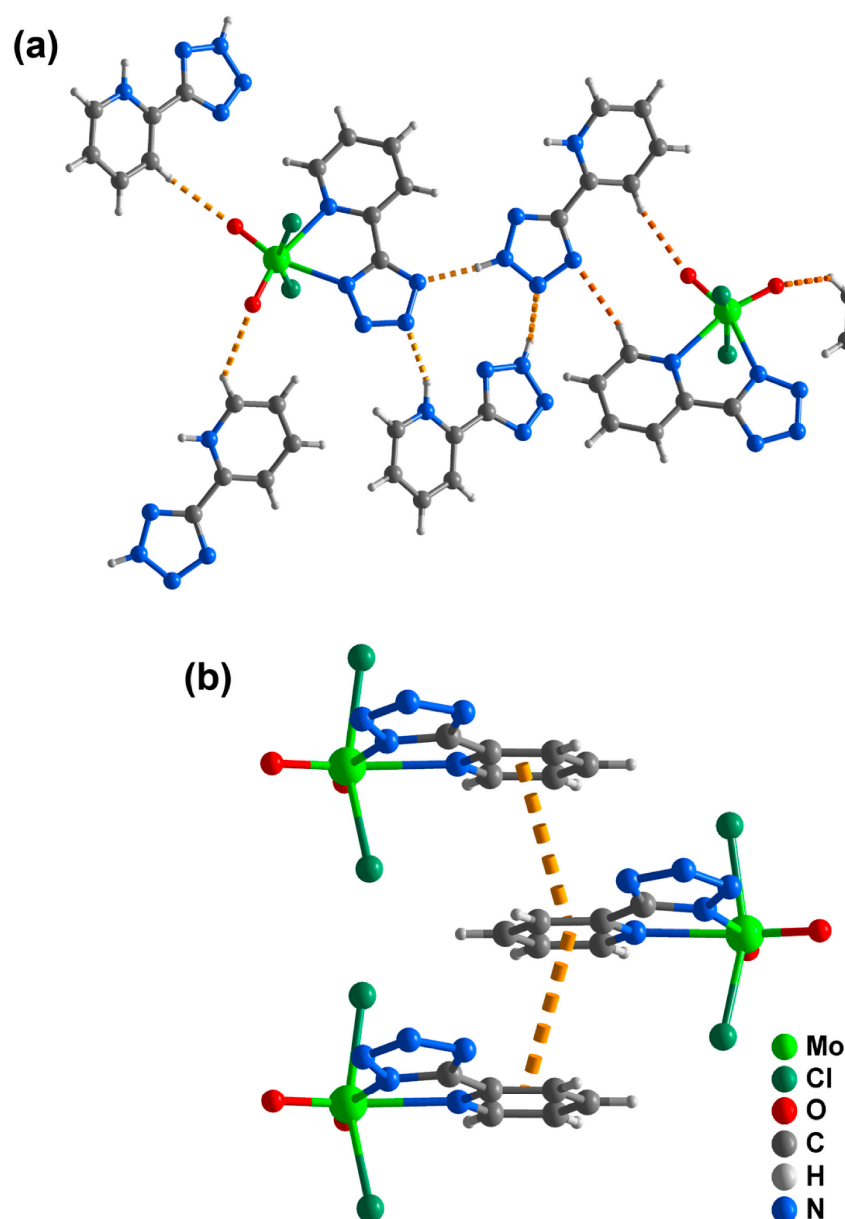


**Figure 3.** Schematic representation of a portion of the crystal packing of **1**, illustrating: (a) the  $\text{N-H}\cdots\text{N}$  and  $\text{C-H}\cdots\text{O}$  hydrogen bonding interactions (dashed orange lines) between the oxido, tetrazole and pyridine rings; (b) the  $\pi$ - $\pi$  interactions (dashed orange lines) between adjacent pyridine rings of coordinated  $\text{pytz}^-$  anionic residues. The atomic labelling was omitted for clarity.



The vibrational spectra of **1** show two bands at  $945 \pm 1 \text{ cm}^{-1}$  (strong in the IR, very strong in the Raman) and  $914\text{--}915 \text{ cm}^{-1}$  (very strong in the IR, medium in the Raman), which are attributed to symmetric and asymmetric Mo=O stretching modes, respectively (Figures 4b and 5b). Another strong IR band at  $338 \text{ cm}^{-1}$  is assigned to  $\nu_{\text{asym}}(\text{Mo-Cl})$ . In the Raman spectrum (Figure 5b), the out-of-plane deformation mode,  $\gamma(\text{MoO}_2)$ , occurs as a medium-intensity band at  $397 \text{ cm}^{-1}$ , and there are several bands in the range  $150\text{--}250 \text{ cm}^{-1}$  that are attributed to  $\nu_{\text{sym}}(\text{Mo-Cl})$  ( $210, 238 \text{ cm}^{-1}$ ) and  $\nu_{\text{sym}}(\text{Mo-N})$  ( $186 \text{ cm}^{-1}$ ) vibrations in accordance with previous assignments for related molybdenum(VI)-pyrazolylpyridine complexes [42].

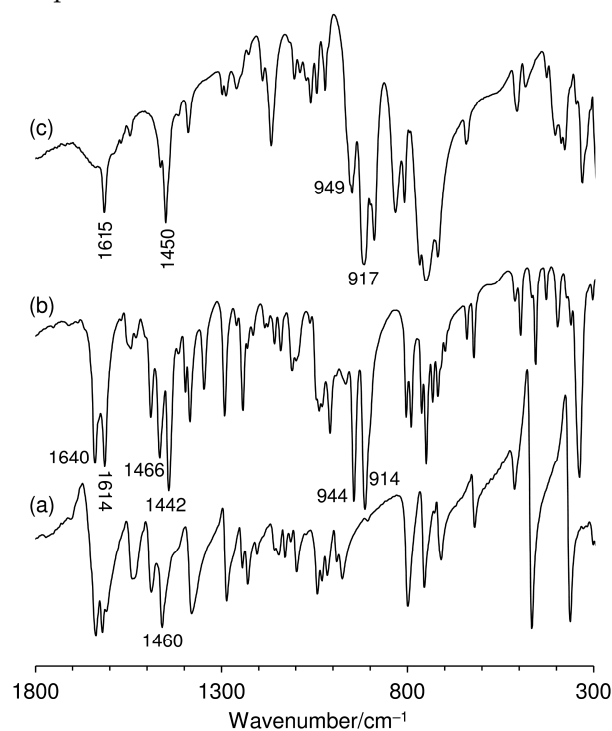


**Figure 4.** FT-IR spectra in the region  $300\text{--}1800 \text{ cm}^{-1}$  of (a) Hpytz, (b) compound **1**, and (c) hybrid **2**.

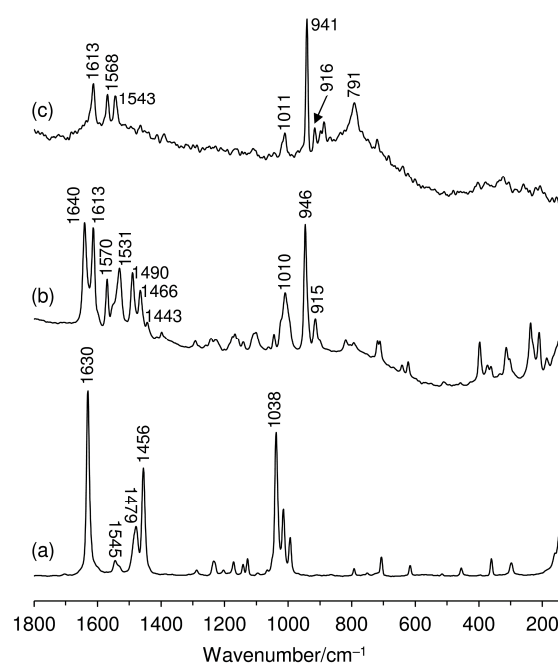


**Figure 5.** Raman spectra in the region  $150\text{--}1800 \text{ cm}^{-1}$  of (a) Hpytz, (b) compound **1**, and (c) hybrid **2**.

The 1000–1700  $\text{cm}^{-1}$  region of the vibrational spectra of **1** contains bands arising from  $\text{H}_n\text{pytz}$  ligand modes. Both the IR and Raman spectra show two strong bands at 1613–1614 and 1640  $\text{cm}^{-1}$ , assigned to pyridyl ring stretching modes [ $\nu(\text{C}=\text{C})$ ] [42,45,46]. The Raman band at 1640  $\text{cm}^{-1}$  is assigned to uncoordinated (charge-balancing) pyridinium-tetrazole ( $\text{H}_2\text{pytz}^+$ ) moieties on the basis that the hybrid polyoxometalate (POM) salt  $(\text{H}_2\text{pytz})_4[\text{SiMo}_{12}\text{O}_{40}] \cdot n\text{H}_2\text{O}$  displays, in the solid-state, a strong band at 1644  $\text{cm}^{-1}$  in the Raman spectrum [47]. Furthermore, an aqueous solution of the salt  $[\text{H}_2\text{pytz}][\text{Cl}]$ , prepared by dissolving  $\text{Hpytz}$  in one equivalent of dilute  $\text{HCl}$ , gives a Raman spectrum containing one pyridyl ring stretching band at 1640  $\text{cm}^{-1}$  [47]. The Raman band at 1614  $\text{cm}^{-1}$  for **1** is attributed to  $N,N$ -coordinated pyridyl-tetrazolate ( $\text{pytz}^-$ ) moieties. Concerning the pair of bands in the IR spectrum, the one at 1640  $\text{cm}^{-1}$  is attributed to the uncoordinated  $\text{H}_2\text{pytz}^+$  cation, while the one at 1614  $\text{cm}^{-1}$  is attributed to both the  $\text{H}_2\text{pytz}^+$  cation and the coordinated  $\text{pytz}^-$  anion. These assignments are supported by the fact that both the POM salt  $(\text{H}_2\text{pytz})_4[\text{SiMo}_{12}\text{O}_{40}] \cdot n\text{H}_2\text{O}$  [47] and the complex salt  $(\text{H}_2\text{pytz})_4[\text{ZnCl}_4]$  [48] display a similar pair of IR bands (1616/1641  $\text{cm}^{-1}$  and 1611/1636  $\text{cm}^{-1}$ , respectively). Furthermore, 5-(2-pyridyl)tetrazolate complexes of various transition metals, in which the  $\text{pytz}^-$  ligand(s) chelate to the metal through the pyridyl and N1 tetrazolate nitrogen atoms, typically display a strong pyridyl ring stretching band at 1605–1615  $\text{cm}^{-1}$  in the IR spectrum, e.g., 1608  $\text{cm}^{-1}$  for  $[\text{Mn}(\text{pytz})_2(\text{H}_2\text{O})_2]$  [19] and 1612  $\text{cm}^{-1}$  for  $[\text{Zn}(\text{pytz})_2(\text{H}_2\text{O})_2]$  [29].

Vibrational bands in the region 1370–1500  $\text{cm}^{-1}$  for **1** are assigned to tetrazole/tetrazolate stretching modes [ $\nu(\text{C}=\text{N})$ ,  $\nu(\text{N}=\text{N})$ ] [45,46]. Focusing on the region 1425–1475  $\text{cm}^{-1}$ , the free ligand  $\text{Hpytz}$  displays one strong  $\nu(\text{tetrazole})$  band in the IR spectrum at 1460  $\text{cm}^{-1}$  (1456  $\text{cm}^{-1}$  in the Raman spectrum) (Figures 4a and 5a), whereas compound **1** gives two strong bands at 1442  $\text{cm}^{-1}$  and 1466  $\text{cm}^{-1}$  (1443 (w)  $\text{cm}^{-1}$  and 1466 (m)  $\text{cm}^{-1}$  in the Raman spectrum). The band at 1442  $\text{cm}^{-1}$  is assigned to  $\nu(\text{tetrazolate})$  and is shifted to lower frequency vs. the free ligand absorption due to deprotonation of the tetrazole group and coordination of the anionic ligand to the  $\text{Mo}^{\text{VI}}$  center in **1**. Very similar  $\nu(\text{tetrazolate})$  stretching frequencies were reported for the aforementioned  $\text{Mn}^{\text{II}}$  and  $\text{Zn}^{\text{II}}$  complexes with  $\text{pytz}^-$  [19,29]. The band at 1466  $\text{cm}^{-1}$  for **1** is attributed to the charge-balancing  $\text{H}_2\text{pytz}^+$  cation, and we note that similar bands were reported previously for the POM salt  $(\text{H}_2\text{pytz})_4[\text{SiMo}_{12}\text{O}_{40}] \cdot n\text{H}_2\text{O}$  (1461–1464  $\text{cm}^{-1}$ ) [47] and the complex salt  $(\text{H}_2\text{pytz})_4[\text{ZnCl}_4]$  (1458  $\text{cm}^{-1}$ ) [48].

The  $^{13}\text{C}\{^1\text{H}\}$  cross polarization (CP) magic-angle spinning (MAS) NMR spectrum of the ligand  $\text{Hpytz}$  shows four broad peaks between 120 and 160 ppm (Figure 6a). These peaks have a clear correspondence with the resonances observed in the solution spectrum ( $\text{DMSO}-d_6$ ;  $\delta = 154.9, 150.1, 143.7, 138.3, 126.1, 122.7$ ) [49–51]. The most downfield-shifted signal at 154.7 ppm in the solid-state spectrum is unambiguously assigned to the tetrazole carbon (Ctz), while the most upfield-shifted peak at 125.7 ppm (with a shoulder at ca. 127.5) is assigned to C3 and C5 of the pyridyl ring. There is some uncertainty regarding whether the peak at 147.5 ppm is due to C2 or C6 of the pyridyl ring (with the asymmetric peak centered at 141.3 ppm being assigned to C4 and C6 or C4 and C2, respectively). Andrews et al. assigned the solution signals at 150.1 and 143.7 ppm to C2 and C6 [50], respectively, while Stagni et al. assigned these resonances contrariwise [51]. We attribute the solid-state NMR peak at 147.5 ppm to C6 (in agreement with Stagni et al.) because the recently developed online calculator CASCADE predicts chemical shifts of 145.4, 149.2, and 155.6 ppm for C2, C6, and Ctz, respectively [52].

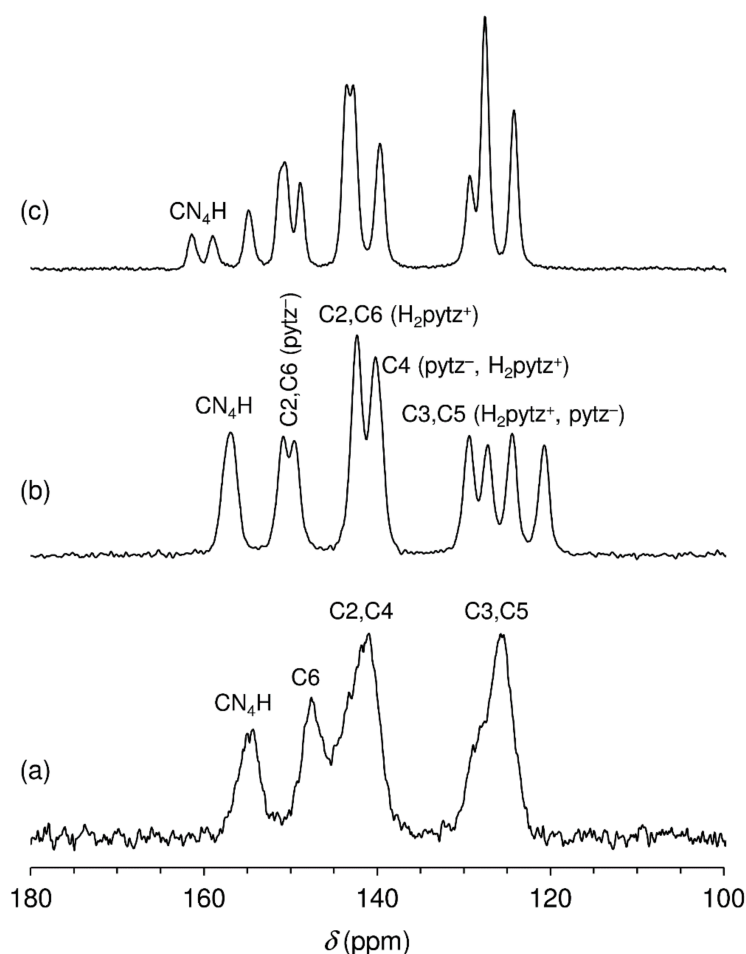


**Figure 6.**  $^{13}\text{C}\{^1\text{H}\}$  cross polarization (CP) magic-angle spinning (MAS) NMR spectra of (a) Hpytz, (b) compound **1**, and (c) hybrid **2**.

In contrast to the free ligand Hpytz, compound **1** displays sharper and better resolved signals in the  $^{13}\text{C}\{^1\text{H}\}$  CP MAS NMR spectrum (Figure 6b). In total, nine distinct peaks are observed, which is consistent with the presence of two different ligand states, i.e., coordinated  $\text{pytz}^-$  and uncoordinated  $\text{H}_2\text{pytz}^+$ . The slightly broader peak at 157.0 ppm is assigned to overlapping Ctz resonances for  $\text{pytz}^-$  and  $\text{H}_2\text{pytz}^+$ . For comparison, the Ctz resonances for the mononuclear complexes  $[\text{La}(\text{pytz})_3(\text{H}_2\text{O})_3]\cdot(\text{H}_2\text{O})_4$  [53] and  $[\text{Ru}(\text{bpy})_2(\text{pytz})](\text{PF}_6)$  ( $\text{bpy} = 2,2'$ -bipyridine) [51] were found at 161.3 and 162.9 ppm, respectively, in the solution  $^{13}\text{C}$  NMR spectra. For metal complexes containing monocoordinated 5-substituted tetrazolates, the Ctz resonance is sensitive to whether binding takes place through N1 or N2 of the five-membered ring. Binding through N1 was previously correlated with a resonance between 151 and 155 ppm, while binding through N2 was correlated with a downfield-shifted resonance between 161 and 165 ppm [51]. Even though the crystal structures for **1** and the  $\text{La}^{\text{III}}$  and  $\text{Ru}^{\text{II}}$  complexes show that the tetrazole ring is N1-coordinated to the metal center, the Ctz resonances appear downfield of the 151–155 ppm range. Stagni et al. attributed this anomalous behavior (for the  $\text{Ru}^{\text{II}}$  complex) to an interannular conjugation effect caused by the coplanarity of the pyridyl and tetrazole rings in the bidentate coordination geometry [51].

The assignment of the remaining resonances in the  $^{13}\text{C}\{^1\text{H}\}$  CP MAS NMR spectrum of **1** was made by reference to the solution NMR spectra reported for  $[\text{La}(\text{pytz})_3(\text{H}_2\text{O})_3]\cdot(\text{H}_2\text{O})_4$  [53] and  $[\text{Ru}(\text{bpy})_2(\text{pytz})](\text{PF}_6)$  [51], which contain chelating  $N(\text{py}),N(\text{tz})$ -coordinated 5-(2-pyridyl)tetrazolate ligands. The two resonances observed at 149.4 and 150.8 are assigned to C2 and C6 of a Mo-coordinated  $\text{pytz}^-$  anion in accordance with the same assignment made for the pair of resonances displayed by the  $\text{La}^{\text{III}}$  and  $\text{Ru}^{\text{II}}$  complexes between 149 and

153 ppm. Towards higher fields, the peaks at 142.3 and 140.2 ppm are attributed to overlapping C2/C6 ( $\text{H}_2\text{pytz}^+$ ) and C4 ( $\text{pytz}^-$ ,  $\text{H}_2\text{pytz}^+$ ) resonances, respectively, while the four resonances between 120 and 130 ppm are assigned to C3 and C5, with the two lower-field ones arising from the pyridinium moiety.

Complexes of the type  $[\text{MoO}_2\text{Cl}_2(\text{L})]$  containing N-heterocyclic aromatic ligands (L) display a rich hydrolysis-condensation-polymerization chemistry. Treatment of various dichloro complexes with water has produced hybrid molybdenum oxide/organic materials with the compositions  $\{[\text{MoO}_3(\text{bpy})][\text{MoO}_3(\text{H}_2\text{O})]\}_n$  [54],  $[\text{Mo}_8\text{O}_{22}(\text{OH})_4(4,4'\text{-di-tert-butyl-2,2'-bipyridine})_4]$  [55],  $[\text{Mo}_2\text{O}_6(\text{HpypzA})]$  (HpypzA = [3-(pyridinium-2-yl)-1H-pyrazol-1-yl]acetate) [56],  $[\text{Mo}_3\text{O}_9(\text{pypz})]_n$  [41],  $[\text{Mo}_2\text{O}_6(2-(1\text{-pentyl-3-pyrazolyl})\text{pyridine})]$  [57], and  $[\text{MoO}_3(2-(2\text{-pyridyl})\text{-benzimidazole})]$  [58]. The reaction of **1** with water was performed under either open reflux conditions for 17 h (method A) or hydrothermal treatment at 100 °C for 19 h in a closed autoclave (method B). Both reactions led to the same microcrystalline product (**2**), as evidenced by matching PXRD patterns (Figure 1d). Compound **2** was also obtained when  $\text{MoO}_3$  was directly reacted with Hpypz in water under open reflux conditions for 3 days (method C).

Microanalyses (C,H,N) and Mo content determination by ICP-OES indicated the empirical formula  $[\text{MoO}_3(\text{Hpypz})]$  for **2**. The presence of a molybdenum oxide microstructure in **2** is indicated by the FT-IR and Raman spectra, which display several  $\nu(\text{Mo}=\text{O})$  bands (887–889, 916–917 and 942–949  $\text{cm}^{-1}$ ) and, in the case of the IR spectrum, broad bands centered at 745 and 833  $\text{cm}^{-1}$  that are assigned to  $\nu(\text{Mo}-\text{O}-\text{Mo})$  vibrational modes (Figures 4c and 5c). In the region 1600–1650  $\text{cm}^{-1}$ , the FT-IR and Raman spectra of **2** show only one band with medium intensity at  $1614 \pm 1 \text{ cm}^{-1}$ , which is exactly coincident with the band displayed by **1** and attributed to  $\nu(\text{C}=\text{C})$  of *N,N*-coordinated pyridyl-tetrazolate ( $\text{pytz}^-$ ) ligands. While compound **1** displays an additional band at  $\sim 1640 \text{ cm}^{-1}$  due to pyridinium moieties, no such band is present for **2**. In the  $\nu(\text{tetrazolate})$  region of the IR spectrum (1425–1475  $\text{cm}^{-1}$ ), compound **2** displays a strong band at 1450  $\text{cm}^{-1}$  and a weaker absorption on the high-frequency side of this band at 1464  $\text{cm}^{-1}$ .

The  $^{13}\text{C}\{^1\text{H}\}$  CP MAS NMR spectrum of **2** shows eleven resolved peaks between 122 and 163 ppm, indicating the presence of two chemically and/or crystallographically distinct  $\text{H}_x\text{pytz}^{(x-1)+}$  moieties in the crystal structure (Figure 6c). This resembles the situation with compound **1** (Figure 6b). An important difference between the two spectra is that compound **2** gives rise to two strongly downfield-shifted Ctz resonances at 158.9 and 161.4 ppm (cf. 157 ppm for **1**). As noted above, Ctz resonances in the range 161–165 ppm have previously been associated with N2-coordination to metal centers, although  $\text{La}^{\text{III}}$  and  $\text{Ru}^{\text{II}}$  complexes with the  $\text{pytz}^-$  anion (with bidentate *N*(py),*N*(N1)-coordination) have been shown to go against this trend by displaying resonances between 161.3 and 162.9 ppm. Nevertheless, the shift of the Ctz resonance from 157.0 ppm for **1** to 161.4 ppm for **2** is significant and may indicate a different coordination mode of the  $\text{pytz}^-$  anion.

There is sparse information in the literature concerning  $^{13}\text{C}$  NMR data for metal coordination compounds containing  $\text{pytz}^-$  ligand(s) that are engaged in chelating (bidentate) and bridging coordination modes. Solution NMR data were reported by Wright et al. for the trinuclear rhenium(I) metallacalix[3]arene  $[\text{Re}(\text{CO})_3(\text{pytz})]_3$  [59], in which the organic ligands adopt a  $\mu_{1,2,4}$  coordination mode [16] ( $\mu_2\text{-}\kappa^2\text{N}1,\text{N}5;\kappa^1\text{N}3$  mode [17]). The non-equivalent  $\text{pytz}^-$  moieties in the  $\text{Re}^{\text{I}}$  complex gave rise to three different patterns in the  $^{13}\text{C}$  NMR spectrum, with the six chemically distinct carbon atoms resonating at about 124.0, 128.5, 142.0, 149.0, 155.5, and 167.0 ppm. Compound **2** displays signals close to these at 124.3, 127.5/129.3, 142.7, 148.8, 154.8, and 161.4, suggesting that the 2-pyridyltetrazolate ligand may be attached to the molybdenum oxide substructure through a similar type of dual chelating/bridging coordination (Figure 7), involving either the pyridyl N-atom, N1 and N3 as in the  $\text{Re}^{\text{I}}$  complex, or possibly the pyridyl N-atom, N1 and N2 ( $\mu_{1,2,3}$  mode) as in, for example, the dinuclear  $\text{Zn}^{\text{II}}$  complex  $[\text{Zn}_2(\text{pytz})_2(\text{H}_2\text{O})_6](\text{CF}_3\text{CO}_2)_2\cdot\text{H}_2\text{O}$  [30]. Complete structural information for **2** is not yet available because attempts to obtain single-crystals suitable for X-ray diffraction have been unsuccessful.

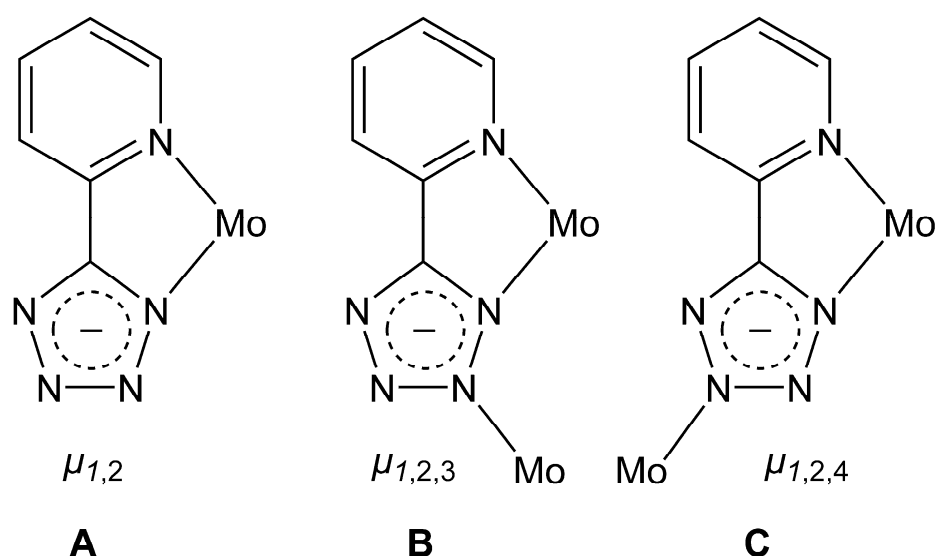


**Figure 7.** (A) The bidentate coordination mode present in complex **1** and (B,C) the dual chelating/bridging modes that may be present in the structure of the hybrid **2**.

## 2.2. Catalytic Studies

### 2.2.1. Model Reaction of *cis*-Cyclooctene Epoxidation

The catalytic performance of **2** was evaluated in the model reaction of *cis*-cyclooctene (Cy8) with *tert*-butyl hydroperoxide (TBHP) at 70 °C, using different types of solvents, namely  $\alpha,\alpha,\alpha$ -trifluorotoluene (TFT) and the bio-based solvents ethanol (EtOH), ethyl acetate (EA), and isobutyl acetate (IBA) (Figure 8). In a 24 h batch run, 91–100% conversion was reached for all solvents, and cyclooctene oxide (Cy8O) was the sole product (100% selectivity). Reactions without oxidant or catalyst were sluggish, leading to less than 14% Cy8 conversion. These results indicate that the simultaneous presence of molybdenum species and oxidant is necessary for the catalytic reaction to occur.

Computational studies of the mechanism of olefin epoxidation in the presence of organo-oxomolybdenum compounds have indicated that the reaction may be initiated via an associative step involving coordination of TBHP to the molybdenum center and the concomitant protonation of an oxo ligand, leading to an intermediate active oxidizing metal species possessing a *tert*-butyl peroxy ligand ( $t\text{BuO}_\beta\text{O}_\alpha^-$ ). The chemical structures of the oxidizing metal species may differ; for example, the  $\text{O}_\beta$  atom of  $t\text{BuO}_\beta\text{O}_\alpha^-$  may interact [60–63] or not [64–67] with the metal center (Figure 9). The nucleophilic attack of the olefin on a peroxy oxygen atom leads to the formation of the corresponding epoxide product and *tert*-butyl alcohol (co-product of TBHP conversion). The chemical structure of the transition state involved in the O-atom transfer step may depend on the type of active oxidizing species (A, B, or C, Figure 9) [60,61,65–67].

The kinetic profiles for the epoxidation of Cy8 using different solvents show that the reaction kinetics was somewhat comparable for TFT and EtOH, and for EA and IBA (Figure 8). The catalytic reaction in TFT or EtOH was faster (85–89% conversion at 5 h) than in EA or IBA (44–48%). The results using EtOH are attractive because EtOH is a readily available bio-based solvent that is an alternative to non-renewable fossil fuel-derived solvents [68]. The catalytic activity of **2** correlates with the dielectric constants of the solvents: TFT (39), EtOH (24.3)  $\gg$  EA (6.4), IBA (5.6) [69].



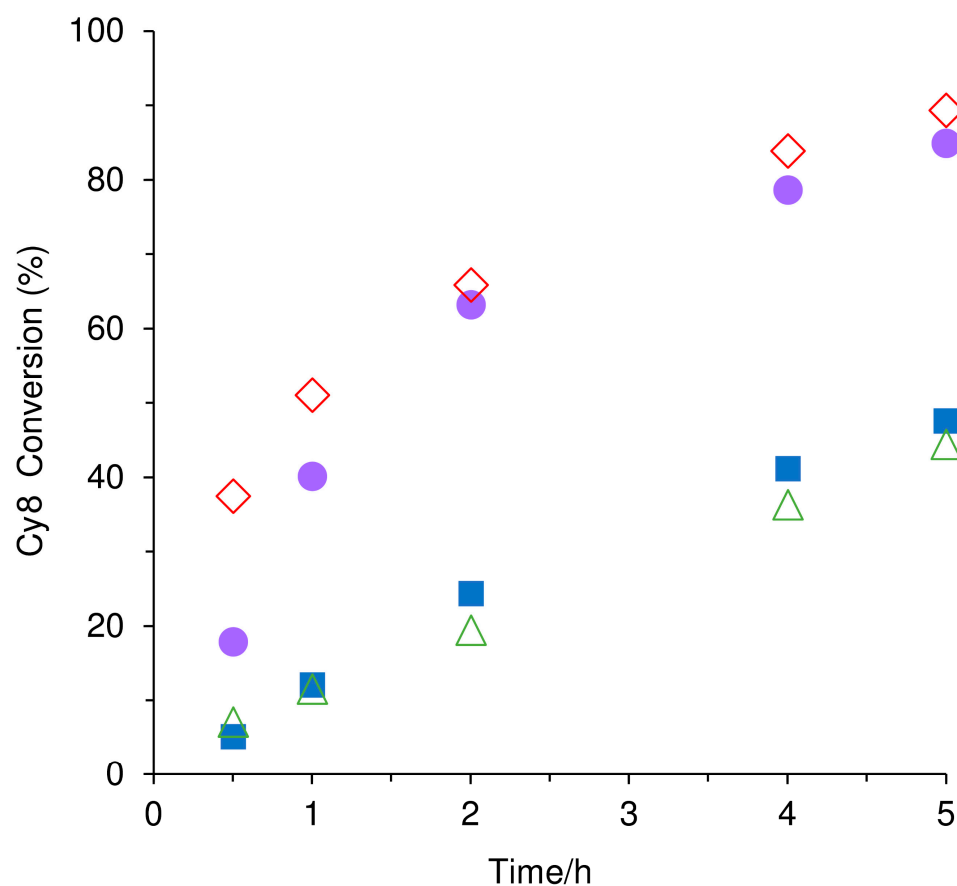


**Figure 8.** Kinetic profiles of the reaction of *cis*-cyclooctene (Cy8) with *tert*-butyl hydroperoxide (TBHP), in the presence of **2**, using  $\alpha,\alpha,\alpha$ -trifluorotoluene (TFT) (◇), ethanol (EtOH) (●), ethyl acetate (EA) (■), or isobutyl acetate (IBA) (△) as solvent, at 70 °C.

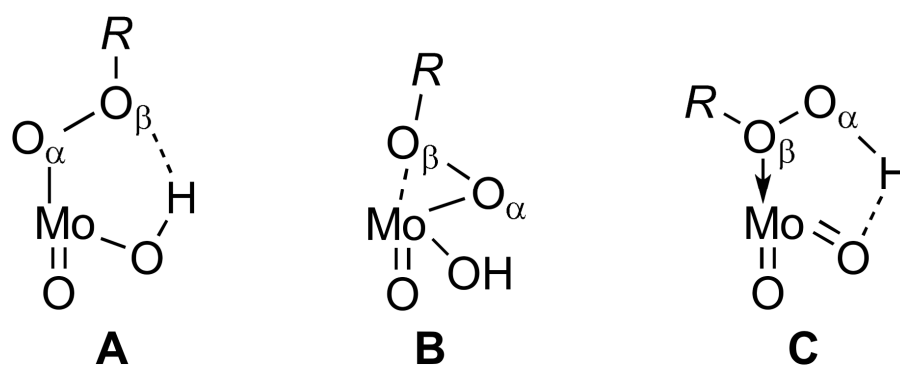


**Figure 9.** Structures of active oxidizing intermediate species reported in the literature for liquid phase catalytic reactions of olefins, in the presence of molybdenum coordination compounds and using hydroperoxide oxidants (R = alkyl or H). The structures differ regarding the absence (A) or presence (B,C) of an interaction between  $O_\beta$  and the metal center.

The reaction mixtures were biphasic liquid-solid for all solvents tested. The solid phase (S) was light blue in color (identical to that for the original catalyst) and the liquid bulk was colorless. The solids were separated from the reaction mixtures (giving 2-S-run1, S = solvent) and characterized by ATR FT-IR spectroscopy and PXRD. The solids 2-S-run1 exhibited similar spectral features (Figure 10a) and PXRD patterns (Figure 10b) to the corresponding data for the original catalyst **2** (only slight differences in the relative intensities of some PXRD reflections were observed). The morphology of particles of **2**

(irregular micron-sized rectangular parallelepipeds) was essentially preserved (Figure 11). Hence, **2** was stable in the different solvent media.

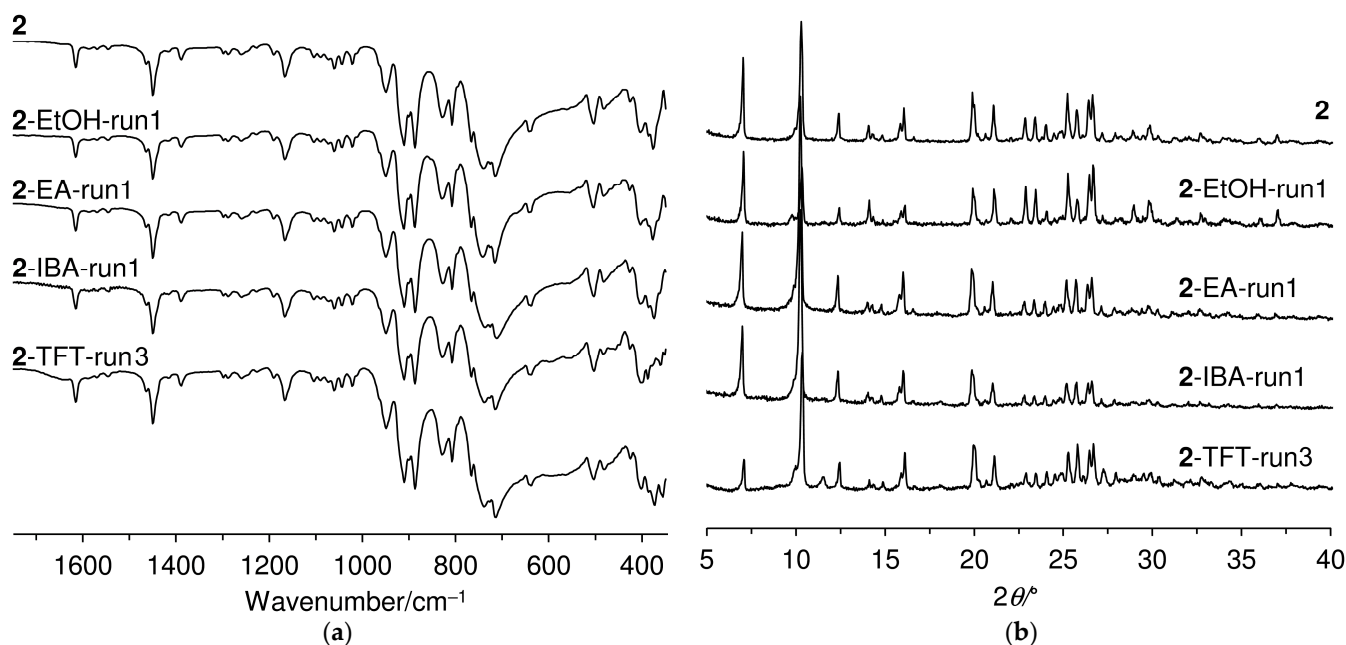


**Figure 10.** (a) ATR FT-IR spectra and (b) PXRD patterns of **2** and the (undissolved) solids separated from the catalytic systems **2**/Cy8/TBHP/solvent.

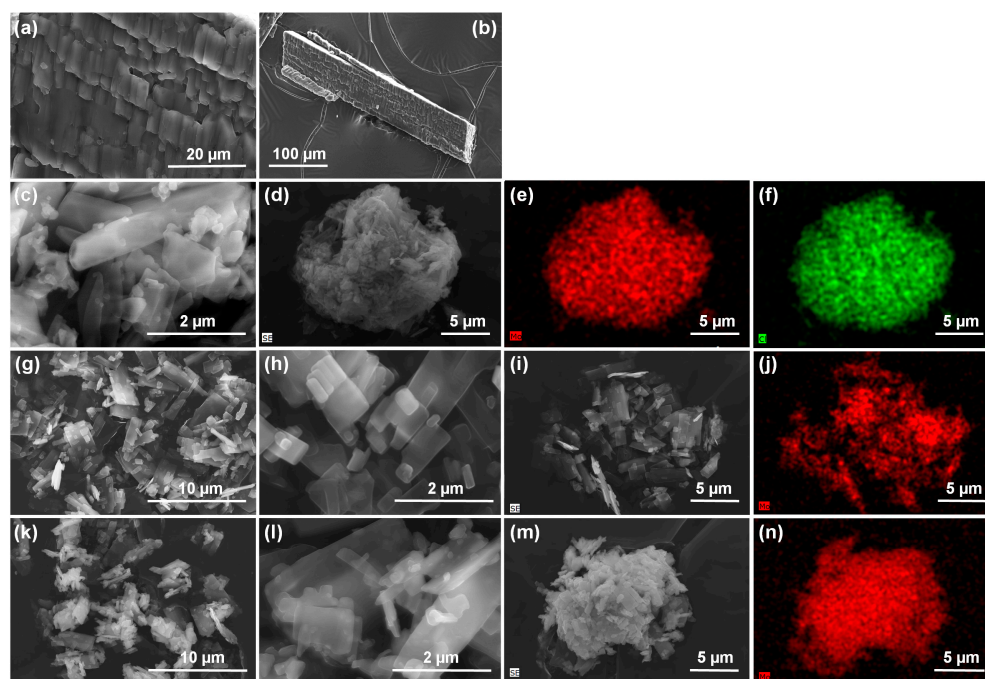


**Figure 11.** SEM images and respective element distribution mappings (in selected cases; Mo (red), Cl (green)) of ligand Hpytz (a,b), **1** (c–f), **2** (g–j), and **2**-TFT-run1 (k–n).

The stability of **2** was further studied by carrying out three consecutive catalytic runs for **2**/Cy8/TBHP/TFT and characterizing the solid recovered after the three runs. The catalyst performed very steadily (Figure 12), and its chemical and structural features were preserved (Figure 10). A leaching test was carried out to check if soluble active species were released from the solid catalyst, accounting for homogeneous catalysis. Specifically, the filtrate (liquid phase) of the leaching test was tested for the homogeneous catalytic

reaction of Cy8 at 70 °C. While the regular catalyst test (i.e., without separating the solid catalyst) led to an increment of conversion of 38% between 1 h and 5 h, the leaching test showed an increment of only 5%, which is approximately equal to that for the blank test performed without catalyst (4% Cy8 conversion in the same time interval). ICP-OES analysis of the leaching test filtrate indicated that the amount of Mo in solution was less than 0.5% of the initial Mo amount in the solid, suggesting that **2** performed essentially as a heterogeneous catalyst.

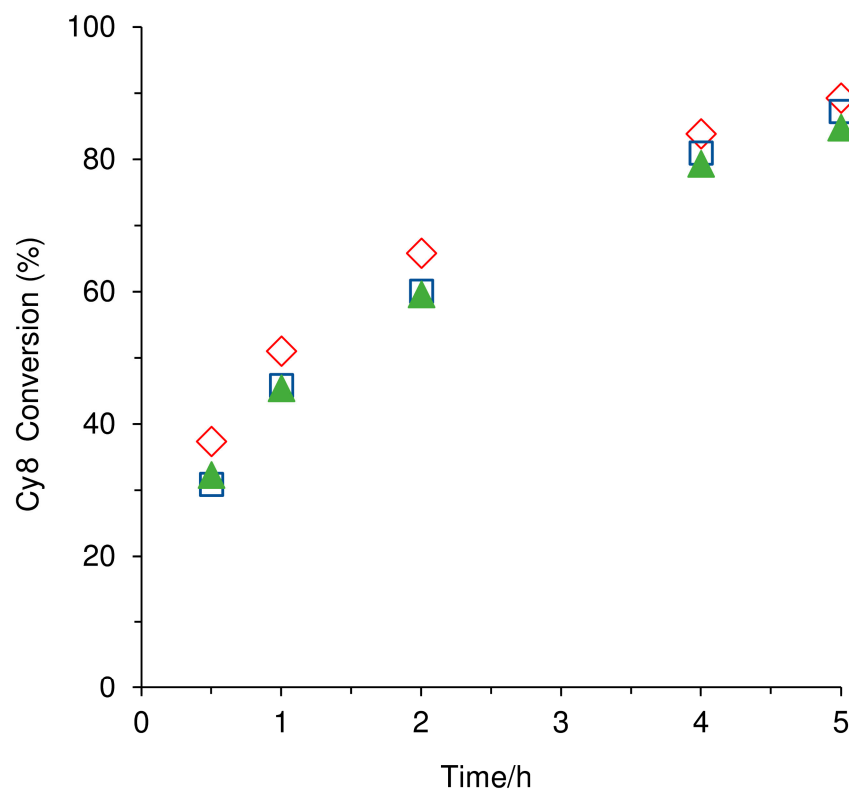


**Figure 12.** Catalyst stability of **2** in consecutive batch runs of Cy8 epoxidation with TBHP in TFT at 70 °C: (◇) run 1, (□) run 2, (▲) run 3.

For reactions performed using TFT as a solvent and a fixed initial Cy8 concentration of 1.0 M, increasing the catalyst:substrate mass ratio from 0.003 to 0.01 led to an increase in the initial reaction rate from 0.5 mmol h<sup>-1</sup> to 1.3 mmol h<sup>-1</sup> (Cy8O selectivity was always 100%). In the studied range of reaction conditions, 100% Cy8 conversion was reached within 24 h. For comparison, the precursor to **2**, compound **1**, displayed very high activity when tested under similar reaction conditions, leading to 98%/100% Cy8O yield at 30 min/1 h, although it performed as a homogeneous catalyst.

Regarding catalysts for olefin epoxidation, only three molybdenum-based compounds that possess organic components containing tetrazole moieties have been reported, namely [Mo<sub>2</sub>O<sub>6</sub>(*m*-trtzH)(H<sub>2</sub>O)<sub>2</sub>] (*m*-trtzH = 5-[3-(1,2,4-triazol-4-ylphenyl)]-1*H*-tetrazole) and [MoO<sub>3</sub>(*p*-trtzH)] (*p*-trtzH = 5-[4-(1,2,4-triazol-4-ylphenyl)]-1*H*-tetrazole), in which only the triazole functionalities of the bitopic ligands partake in coordination to Mo<sup>VI</sup> centers [70], and the POM salt (H<sub>2</sub>pytz)<sub>4</sub>[SiMo<sub>12</sub>O<sub>40</sub>]·*n*H<sub>2</sub>O, containing a non-coordinated pyridinium-tetrazole counterion [47]. Under similar reaction conditions, the activity of the POM salt (acting as a homogeneous catalyst) was slightly inferior to that of **2** (84% conversion at 6 h vs. 89% at 5 h, respectively), while the hybrids [Mo<sub>2</sub>O<sub>6</sub>(*m*-trtzH)(H<sub>2</sub>O)<sub>2</sub>] and [MoO<sub>3</sub>(*p*-trtzH)] displayed significantly lower activity (21% and 30% conversion at 6 h, respectively).

The discovery of new hybrid organomolybdenum heterogeneous catalysts has received limited attention despite the considerable practical interest of obtaining catalysts that are easier to recover and reuse and display enhanced productivity. Table 1 lists the studies reported in the literature for bulk organo-molybdenum heterogeneous epoxida-

tion catalysts [40,54,56,71–77]. Rigorous comparisons between **2** and literature studies are difficult due to the diverse reaction conditions used (temperature, solvent, concentrations of reactants, reaction time, etc.). The results for **2** seem to compare favorably with those reported for the hybrid  $[\text{MoO}_3(\text{biim})]$  (biim = 2,2'-biimidazole) tested under similar reaction conditions, which led to 83%/99% Cy8 conversion at 6 h/24 h (entries 1 and 10, Table 1) [71]. At a lower temperature (55 °C), the octanuclear complex  $[\text{Mo}_8\text{O}_{24}(\text{pypzEA})_4]$ , where pypzEA = ethyl[3-(pyridin-2-yl)-1*H*-pyrazol-1-yl]acetate, led to 89%/100% Cy8 conversion at 6 h/24 h (entries 1 and 4, Table 1) [40]. The reaction kinetics were faster in the presence of *cis*-dioxomolybdenum(VI)-amino acid containing compounds, which led to complete conversion at 1 h/50 °C, using chloroform as solvent and 2 mol% molybdenum relative to olefin (entries 1 and 17, Table 1) [76]. A Schiff base polyoxometalate nanohybrid, synthesized by the reaction of  $[\text{PMo}_{11}\text{O}_{39}]^{7-}$ ,  $[\text{MoO}_2(\text{acac})_2]$ , and ethylenediamine, led to almost complete conversion at 30 min, but required a higher reaction temperature (reflux conditions using 1,2-dichloroethane (DCE) as solvent) and a higher amount of molybdenum (*ca.* 8 mol% relative to the substrate, compared to 1 mol% Mo for **2**; entries 1 and 18, Table 1) [77]. For  $(\text{Himi})_4(\text{imi})_2(\text{Mo}_8\text{O}_{26})$  (imi = imidazole) and using a higher amount of molybdenum (5 mol%), at 45 °C, 97% conversion was reached after 12 h (entry 16, Table 1) [75]. Several catalysts listed in Table 1 performed steadily in consecutive batch runs, although, for example,  $[\text{piperazinCH}_2\{\text{MoO}_2(\text{Salen})\}]_n$  suffered metal leaching (entry 13) [74].

**Table 1.** Catalytic results for **2** and literature data for bulk heterogeneous hybrid Mo catalysts, tested for *cis*-cyclooctene (Cy8) epoxidation with *tert*-butyl hydroperoxide (TBHP).

Entry	Catalyst <sup>a</sup>	Reaction Conditions <sup>b</sup>			Conv. (%) <sup>c</sup>	Sel. (%) <sup>d</sup>	Ref.
		Solv./T (°C)	Mo: Cy8: TBHP	t/h			
1	<b>2</b>	TFT/70	1:100:152	5/24	c <sub>1</sub> -89/100 c <sub>2</sub> -87/100 c <sub>3</sub> -85/100	c <sub>1</sub> -100/100 c <sub>2</sub> -100/100 c <sub>3</sub> -100/100	This work
2		EtOH/70	1:100:152	5/24	85/100	100/100	
3	$[\text{Mo}_4\text{O}_{12}(\text{pypz})_4]$	-/55	1:100:152	6/24	c <sub>1</sub> -55/92 c <sub>2</sub> -57/89	c <sub>1</sub> -100/100 c <sub>2</sub> -100/100	[40]
4	$[\text{Mo}_8\text{O}_{24}(\text{pypzEA})_4]$	-/55	1:100:152	6/24	c <sub>1</sub> -89/100 c <sub>2</sub> -91/100	c <sub>1</sub> -100/100 c <sub>2</sub> -100/100	[40]
5	$[\text{Mo}_2\text{O}_6(\text{HpypzA})]$	decane/55	1:100:152	24	26	100	[56]
6		hexane/55	1:100:152	24	24	100	
7		DCE/55	1:100:152	24	74	100	
8	$\{[\text{MoO}_3(\text{bpy})][\text{MoO}_3(\text{H}_2\text{O})]\}_n$	hexane/55	1:50:76	24/48	c <sub>1</sub> -22/34 c <sub>2</sub> --38/~50 c <sub>3</sub> --30/~45 c <sub>4</sub> --30/~45	c <sub>1</sub> -100/100 c <sub>2</sub> -100/100 c <sub>3</sub> -100/100 c <sub>4</sub> -100/100	[54]
9		hexane/75	1:50:76	6	45	100	
10	$[\text{MoO}_3(\text{biim})]$	TFT/70	1:100:153	6/24	c <sub>1</sub> -83/99 c <sub>2</sub> -87/- c <sub>3</sub> -99/-	c <sub>1</sub> -100/100 c <sub>2</sub> -100/- c <sub>3</sub> -100/-	[71]
11	$[\text{MoO}_2(\text{Naph-His})]$	$\text{CCl}_4/\text{reflux}$	1:174:244	8	c <sub>1</sub> -100 c <sub>2</sub> -100 c <sub>3</sub> -100 c <sub>5</sub> -98	c <sub>1</sub> -100 c <sub>2</sub> -100 c <sub>3</sub> -100 c <sub>5</sub> -100	[72]
12	MoL <sup>1</sup> -nano, MoL <sup>2</sup> -nano	$\text{CHCl}_3/45$	- <sup>e</sup>	1	MoL <sup>1</sup> -nano: c <sub>1</sub> -100 c <sub>2</sub> -100 c <sub>3</sub> -97 c <sub>4</sub> -94 c <sub>5</sub> -93 MoL <sup>2</sup> -nano: c <sub>1</sub> -100 c <sub>2</sub> -100 c <sub>3</sub> -99 c <sub>4</sub> -98 c <sub>5</sub> -97	MoL <sup>1</sup> -nano: c <sub>1</sub> -100 c <sub>2</sub> -100 c <sub>3</sub> -100 c <sub>4</sub> -100 c <sub>5</sub> -100 MoL <sup>2</sup> -nano: c <sub>1</sub> -100 c <sub>2</sub> -100 c <sub>3</sub> -100 c <sub>4</sub> -100 c <sub>5</sub> -100	[73]

Table 1. Cont.

Entry	Catalyst <sup>a</sup>	Reaction Conditions <sup>b</sup>			Conv. (%) <sup>c</sup>	Sel. (%) <sup>d</sup>	Ref.
		Solv./T (°C)	Mo: Cy8: TBHP	t/h			
13	[piperazinCH <sub>2</sub> {MoO <sub>2</sub> (Salen)}]	DCE/75	1:200:200	c <sub>1</sub> -12	c <sub>1</sub> -95	c <sub>1</sub> -98	[74]
				c <sub>2</sub> -7	c <sub>2</sub> -98	c <sub>2</sub> -98	
				c <sub>3</sub> -5	c <sub>3</sub> -99	c <sub>3</sub> -98	
				c <sub>4</sub> -4	c <sub>4</sub> -97	c <sub>4</sub> -98	
14	[piperazinCH <sub>2</sub> {MoO <sub>2</sub> (Salophen)}]	DCE/75	1:200:200	c <sub>5</sub> -4	c <sub>5</sub> -98	c <sub>5</sub> -98	
				12	89	97	
15	[piperazinCH <sub>2</sub> {MoO <sub>2</sub> (Salpn)}]	DCE/75	1:200:200	12	93	97	
16	(Himi) <sub>4</sub> [(imi) <sub>2</sub> (Mo <sub>8</sub> O <sub>26</sub> )]·H <sub>2</sub> O	DCE/35	1:21:21	12	c <sub>1</sub> -97	c <sub>1</sub> -100	[75]
					c <sub>2</sub> ~97	c <sub>2</sub> -100	
					c <sub>3</sub> ~97	c <sub>3</sub> -100	
					c <sub>4</sub> ~97	c <sub>4</sub> -100	
					c <sub>5</sub> ~97	c <sub>5</sub> -100	
17	[Mo <sub>2</sub> O <sub>4</sub> (OH) <sub>4</sub> (AA)]	DCE/50	1:50:100	1	For Gly catalyst:	100	[76]
					c <sub>2</sub> -96		
					c <sub>3</sub> -96		
					99	c <sub>1</sub> - ≥ 99	
18	nanohybrid Schiff base POM	DCE/reflux	1:13:29	0.5	c <sub>2</sub> to c <sub>5</sub> -93-99	c <sub>2</sub> - ≥ 99	[77]
						c <sub>3</sub> - ≥ 99	
						c <sub>4</sub> - ≥ 99	
						c <sub>5</sub> - ≥ 99	

<sup>a</sup> pypz = 2-[3(5)-pyrazolyl]pyridine, pypzEA = ethyl[3-(pyridin-2-yl)-1H-pyrazol-1-yl]acetate, HpypzA = [3-(pyridinium-2-yl)-1H-pyrazol-1-yl]-acetate, bpy = 2,2'-bipyridine, biim = 2,2'-biimidazole, Naph = 2-hydroxy-1-naphthaldehyde, His = L-histidine, MoL<sup>n</sup>-nano = nanosized [MoO<sub>2</sub>(L)] catalysts with Schiff base ligands derived from 2,2'-dimethylpropylenediamine (H<sub>2</sub>L<sup>1</sup>) or 1,2-cyclohexanediamine (H<sub>2</sub>L<sup>2</sup>), Salen = *N,N'*-ethylenebis(salicylideneamine), Salophen = *N,N'*-phenylenebis(salicylideneamine), Salpn = *N,N'*-propylenebis(salicylideneamine), imi = imidazole, AA = Met (L-methionine), phe (L-phenylalanine), dmPhe (*N,N*-dimethyl-l-phenylalanine), Gly (glycine) and Pro (L-proline). <sup>b</sup> Solv. = solvent, T = reaction temperature, t = reaction time, TFT =  $\alpha,\alpha,\alpha$ -trifluorotoluene, DCE = 1,2-dichloroethane. <sup>c</sup> Conversion of Cy8; c<sub>i</sub> = catalytic run i (i = 1, 2, 3, 4, ...). <sup>d</sup> Epoxide selectivity; c<sub>i</sub> = catalytic run i (i = 1, 2, 3, 4, ...). <sup>e</sup> 1 mol% catalyst relative to olefin (Mo loading not specified).

### 2.2.2. Epoxidation of Biomass-Derived Olefins

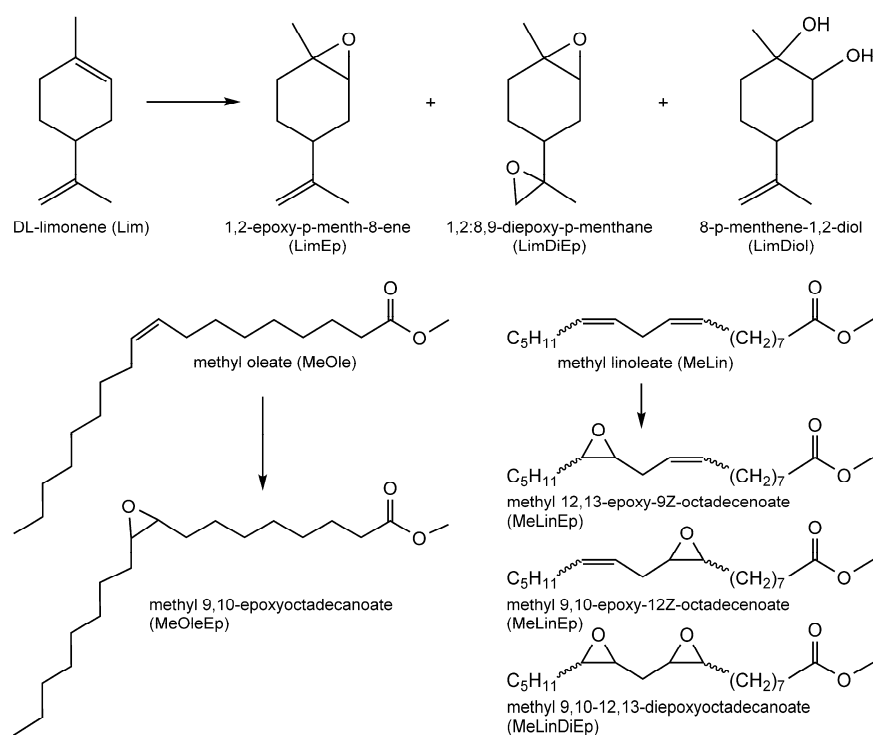
Catalyst **2** was further explored for the epoxidation of bio-based olefins to valuable bioproducts with potential to replace/complement petrochemicals. The biobased olefins tested were the fatty acid methyl esters (FAMEs) methyl oleate (MeOle) and methyl linoleate (MeLin), and the terpene *DL*-limonene (Lim) (Scheme 1), using TBHP as oxidant and TFT as solvent at 70 °C (Figure 13, Table 2).

Table 2. Catalytic results for **2** and [MoO<sub>3</sub>(biim)] in the epoxidation of bio-derived olefins.

Entry	Catalyst	Reaction Conditions <sup>a</sup>			Conv. (%) <sup>b</sup>	Sel. (%) <sup>c</sup>	Ref.
		Olefin	Mo:olefin:TBHP	t/h			
1	<b>2</b>	MeOle	1:100:210	5/24	85/100	100/100	This work
2	-	MeLin	1:100:210	5/24	67/86	86/66(0.2/0.5)	
3	-	Lim	1:100:210	5/24	100/100	73/51(0.3/0.3)	
4	[MoO <sub>3</sub> (biim)]	MeOle	1:100:226	6/24	72/97	99/97	[71]
5	-	MeLin	1:100:226	6/24	66/88	86/65(0.2/0.5)	
6	-	Lim	1:100:226	6/24	97/100	80/55(0.2/0.6)	

<sup>a</sup> In TFT at 70 °C. <sup>b</sup> Olefin conversion at 5 h/24 h or 6 h/24 h, depending on the catalyst. <sup>c</sup> Total selectivity to monoepoxides at 5 h/24 h or 6 h/24 h (depending on the catalyst). Within parentheses are the molar ratios of diepoxide/monoepoxide compounds at 5 h/24 h or 6 h/24 h (depending on the catalyst), in the case of Lim and MeLin.





**Scheme 1.** Epoxidation of biomass-derived olefins to useful bio-based products.

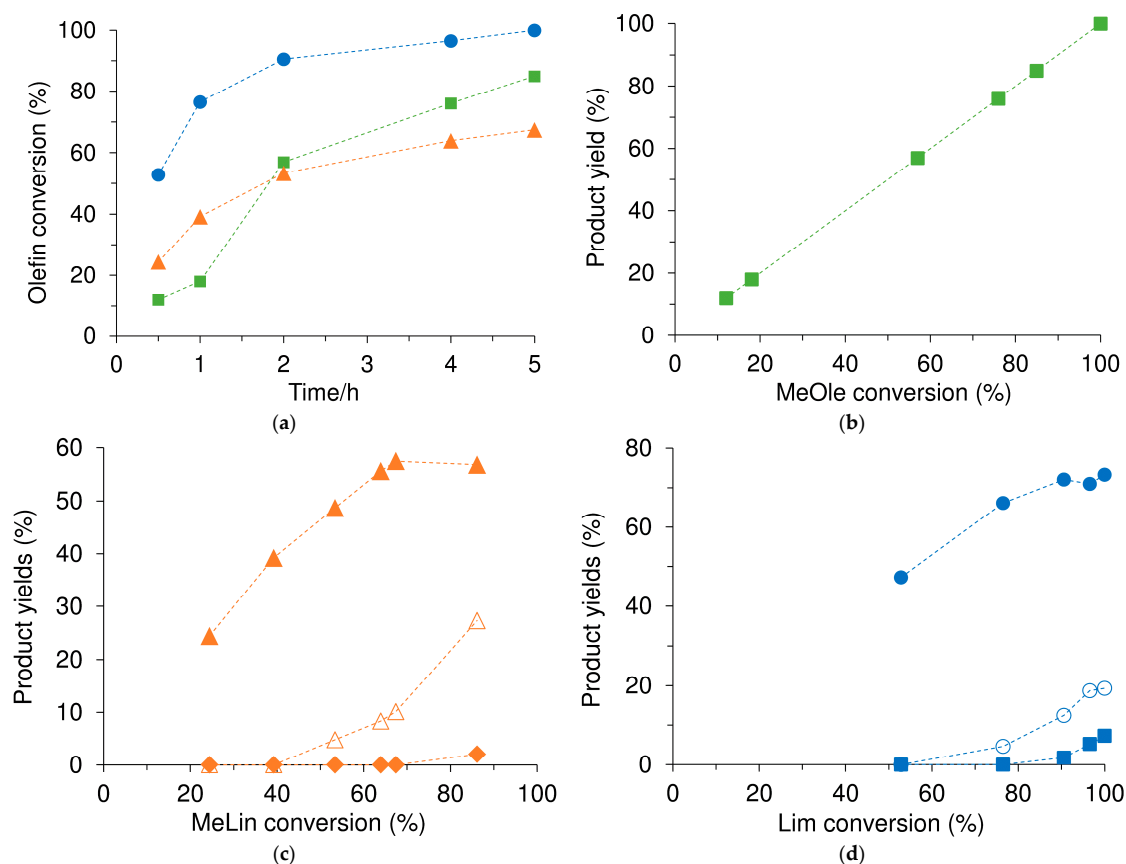


**Figure 13.** (a) Kinetic profiles of the reactions of MeOle (■), MeLin (▲), and Lim (●) in the presence of **2**. Respective product yields: (b) MeOle reaction—MeOleEp (■); (c) MeLin reaction—MeLinEp (▲), MeLinDiEp (△), and cyclization products (◆); (d) Lim reaction—LimEp (●), LimDiEp (○), and LimDiol (■).

MeOle and MeLin can be obtained by the transesterification of vegetable oils such as olive, palm, rapeseed, corn, sesame, soybean, and sunflower [78–80]. The epoxidized vegetable oils/FAMES may be used as solvents in the cosmetic and pharmaceutical industries, as reactive diluents [81], PVC plasticizers and stabilizers [79,82,83], in detergents [84] and UV-curable coatings [85], and to produce biodegradable lubricants [86,87] and polyols, which are important raw materials for the synthesis of polyesters and polyurethanes [79,88–90].

The reaction of MeOle gave the monoepoxide methyl 9,10-epoxyoctadecanoate (MeOleEp) as the sole product in 85%/100% yield at 5 h/24 h. The reaction of MeLin was slower: 67%/86% conversion at 5 h/24 h. The monoepoxides methyl 12,13-epoxy-9Z-octadecenoate and methyl 9,10-epoxy-12Z-octadecenoate (MeLinEp) were the predominant products, formed in equimolar amounts with a total yield of 57% at 24 h, suggesting a similar regioselectivity towards the epoxidation of the 9,10 and 12,13 C=C double bonds. The MeLinEp selectivity decreased with time, from 100% at 30 min to 66% at 24 h, which was accompanied by the formation of the diepoxide diastereoisomers of methyl 9,10,12,13-diepoxyoctadecanoate (MeLinDiEp) and the regioisomers of the hydroxytetrahydrofuran derivatives methyl 10,13-dihydroxy-9,12-epoxy-octadecanoate and methyl 9,12-dihydroxy-10,13-epoxy-octadecanoate, in yields of 27% and 2%, respectively, at 24 h. The MeLinDiEp/MeLinEp molar ratio was 0.5 at 24 h. The hydroxytetrahydrofuran products may be formed via intramolecular cyclization of epoxydiol intermediates, which may be relatively unstable due to the proximity of the diol and epoxy ring in the molecule (separated by a methylene group) [91–94].

Lim is a cyclic terpenic diene found in citrus oils. The corresponding epoxide products, namely 1,2-epoxy-p-menth-8-ene (LimEp) and 1,2:8,9-diepoxyp-menthane (LimDiEp), have wide application potential. LimEp has been employed in metal coatings, varnishes, and printing inks [79], and in the synthesis of fragrances [95,96], pharmaceuticals [97] and food additives, biodegradable polycarbonates (by copolymerization with CO<sub>2</sub>) [98], and polyesters (by copolymerization with cyclic anhydrides) [99]. LimDiEp is used as a solvent and in epoxy resins as a reactive diluent, within a large spectrum of applications [100]. The system LimDiEp/CO<sub>2</sub> gives non-isocyanate polyurethanes and thermosetting polymers [101–103].

The reaction of Lim was complete at 5 h (Figure 13a, Table 2). The selectivity to the diastereoisomers (*cis* and *trans*) of LimEp decreased from 90% at 53% conversion (30 min) to 73% at 100% conversion (5 h), due to the formation of the diepoxide isomers LimDiEp and LimDiol (19% and 7% yield (or selectivity), respectively, at 5 h). Some byproducts seemed to be formed via allylic oxidation, although they were not clearly identified. The reaction is regioselective towards the epoxidation of the endocyclic C=C double bond rather than the exocyclic one, because 8,9-epoxy-p-menth-1-ene (exocyclic oxide) was not detected, and the mole ratio of LimDiEp/LimEp was 0.3 at 24 h.

To the best of our knowledge, there is only one report of a bulk organomolybdenum heterogeneous catalyst tested in the epoxidation of these bio-derived olefins (Table 2, entries 4–6) [71]. Based on olefin conversion at 5–6 h, the polymeric hybrid [MoO<sub>3</sub>(biim)] compares unfavorably with **2**, under almost identical reaction conditions. Broadening the comparison to homogeneous catalysts possessing tetrazole components, the catalyst (H<sub>2</sub>pytz)<sub>4</sub>[SiMo<sub>12</sub>O<sub>40</sub>]·*n*H<sub>2</sub>O led to similar results to **2** in the reaction of MeOle (88%/100% conversion at 6 h/24 h, and MeOleEp was the only product), but to superior results in the reaction of MeLin (87%/100% conversion at 6 h/24 h) [47]. The two olefins were tested at 70 °C using a Mo:olefin:oxidant molar ratio of 1:100:250. The cyclization products were the main products of the MeLin reaction (40% selectivity at 24 h); MeLinEp and MeLinDiEp were formed in 28 and 33% selectivity, respectively, at 100% conversion. With Lim as a substrate, (H<sub>2</sub>pytz)<sub>4</sub>[SiMo<sub>12</sub>O<sub>40</sub>]·*n*H<sub>2</sub>O led to LimEp and LimDiEp in 28% and 6% selectivity, respectively, at 85% conversion, 24 h, and 36% LimDiol selectivity, indicating that it possessed activity for epoxide ring-opening reactions.

### 3. Materials and Methods

#### 3.1. General Considerations

All preparations and manipulations were carried out under nitrogen using standard Schlenk techniques. The following chemicals were purchased from Sigma-Aldrich (St. Louis, MO, USA), unless otherwise stated, and used as received: molybdenum(VI) dichloride dioxide, anhydrous tetrahydrofuran (99%), hexane ( $\geq 99\%$ , Carlo Erba, Milan, Italy), acetone ( $\geq 99.5\%$ ), diethyl ether ( $\geq 99.8\%$ ), ethyl acetate (99.9%), isobutyl acetate (99%), anhydrous  $\alpha, \alpha, \alpha$ -trifluorotoluene ( $\geq 99\%$ ), anhydrous ethanol (99.9%, Carlo Erba), *cis*-cyclooctene (95%, Alfa Aesar), methyl oleate (MeOle, 99%), methyl linoleate (MeLin, 95%, Alfa Aesar, Ward Hill, MA, USA), *DL*-limonene (Lim,  $>95\%$ , Merck, Kenilworth, NJ, USA), 5.5 M *tert*-butyl hydroperoxide in decane, and the internal standards methyl decanoate (99%) and undecane ( $>99\%$ ). A literature procedure was used to prepare the ligand 5-(2-pyridyl)-1*H*-tetrazole [47].

CHN microanalyses were performed using a Leco TruSpec 630-200-200 analyzer (Leco, Saint Joseph, MI, USA). Mo was determined by ICP-OES at the Central Laboratory of Analysis, University of Aveiro. FT-IR spectra (KBr discs) were collected in the range 4000–300  $\text{cm}^{-1}$  using a Unicam Mattson 7000 spectrophotometer (Mattson Instruments Inc., Madison, WI, USA) equipped with a DTGS CsI detector (resolution 4  $\text{cm}^{-1}$ , 128 scans). Attenuated total reflectance (ATR) FT-IR spectra were measured on a Bruker Tensor 27 spectrometer (Bruker, Billerica, MA, USA) equipped with a Specac Golden Gate Mk II ATR accessory (Specac, Orpington, UK) having a diamond top plate and KRS-5 focusing lenses (resolution 4  $\text{cm}^{-1}$ , 256 scans). FT-Raman spectra were recorded in the range 4000–50  $\text{cm}^{-1}$  on a RFS-100 Bruker FT-Spectrometer equipped with a Nd:YAG laser with an excitation wavelength of 1064 nm (resolution 4  $\text{cm}^{-1}$ , 500 scans).  $^1\text{H}$  NMR spectra were recorded in  $\text{DMSO-d}_6$  with a Bruker Avance 300 spectrometer (300.13 MHz). Solid-state  $^{13}\text{C}\{^1\text{H}\}$  CP MAS NMR spectra were recorded using a Bruker AVANCE III—400 MHz spectrometer with an ultrashielded static magnetic field of 100.61 MHz. The spectra were recorded with 3.2  $\mu\text{s}$   $^1\text{H}$  90° pulses, 3.5 ms contact time, spinning rate of 12 kHz, and 5 s recycle delays. Chemical shifts are quoted in ppm from TMS. PXRD data were collected at room temperature on a Malvern Panalytical Empyrean diffractometer (Malvern Panalytical, Malvern, UK) equipped with a spinning flat sample holder and a PIXcel 1D detector set at 240 mm from the sample, in a Bragg-Brentano para-focusing optics configuration.  $\text{Cu-K}_{\alpha 1,2}$  X-radiation ( $\lambda_1 = 1.540598 \text{ \AA}$ ,  $\lambda_2 = 1.544426 \text{ \AA}$ ) filtered with a nickel foil was used. Samples were step-scanned from 3 to 70° ( $2\theta$ ) in 0.02°  $2\theta$  steps with a counting time of 50 s per step. SEM images, EDS analysis, and elemental (Mo, Cl) mappings were obtained on a Hitachi SU-70 microscope (Hitachi High-Tech Europe GmbH, Krefeld, Germany) equipped with a Bruker Quantax 400 detector at 15 kV. Samples were prepared by deposition on aluminum sample holders followed by carbon coating using an Emitech K 950 carbon evaporator (Emitech SAS, Montigny-le-Bretonneux, France).

#### 3.2. Synthesis of $(\text{H}_2\text{pytz})[\text{MoO}_2\text{Cl}_2(\text{pytz})]$ (1)

$\text{MoO}_2\text{Cl}_2$  (0.50 g, 2.51 mmol) was dissolved in anhydrous THF (20 mL), and the mixture was stirred at 50 °C for 20 min. The resulting clear blue solution was added to  $\text{Hpytz}$  (0.74 g, 5.02 mmol) and left to stir at room temperature for 4 h. After concentrating the resultant solution, hexane (20 mL) was added to precipitate a white solid, which was washed with diethyl ether ( $2 \times 20 \text{ mL}$ ) and vacuum-dried at room temperature. Yield: 1.09 g, 88%. Anal. Calcd. for  $\text{C}_{12}\text{H}_{10}\text{Cl}_2\text{MoN}_{10}\text{O}_2$ : C, 29.23; H, 2.04; N, 28.40. Found: C, 28.91; H, 2.12; N, 28.19. FT-IR (KBr,  $\text{cm}^{-1}$ ): 3089 (m), 3058 (w), 1640 (vs), 1614 (vs), 1544 (w), 1530 (m), 1490 (s), 1466 (vs), 1442 (vs), 1416 (w), 1397 (m), 1385 (s), 1347 (m), 1292 (s), 1242 (s), 1230 (w), 1215 (w), 1158 (m), 1140 (m), 1110 (m), 1099 (sh), 1037 (m), 1009 (s), 944 (s), 914 (vs), 803 (s), 790 (vs), 762 (m), 749 (vs), 732 (m), 718 (m), 698 (w), 640 (m), 621 (s), 510 (w), 496 (m), 455 (s), 427 (w), 396 (m), 372 (w), 360 (m), 338 (vs), 301 (w). Raman ( $\text{cm}^{-1}$ ): 3087 (w), 3071 (w), 1640 (vs), 1613 (vs), 1570 (m), 1531 (m), 1490 (m), 1466 (m), 1443 (w), 1398 (w), 1292 (w), 1243 (w), 1232 (w), 1168 (w), 1142 (w), 1102 (w), 1045 (w),

1010 (m), 946 (vs), 915 (m), 819 (w), 719 (w), 711 (w), 641 (w), 621 (w), 397 (m), 373 (w), 362 (w), 314 (m), 238 (m), 210 (m), 186(w), 116 (s).  $^{13}\text{C}\{^1\text{H}\}$  CP MAS NMR:  $\delta = 157.0$  ( $\text{CN}_4$ ), 150.8, 149.4 (C2,C6 (pytz<sup>-</sup>)), 142.3 (C2,C6 ( $\text{H}_2\text{pytz}^+$ )), 140.2 (C4 (pytz<sup>-</sup>,  $\text{H}_2\text{pytz}^+$ )), 129.4, 127.3 (C3,C5 ( $\text{H}_2\text{pytz}^+$ )), 124.4, 120.7 (C3,C5 (pytz<sup>-</sup>)) ppm. Crystals of **1** suitable for X-ray analysis (identified as ( $\text{H}_2\text{pytz}$ )[ $\text{MoO}_2\text{Cl}_2(\text{pytz})$ ]) were obtained by slow diffusion of diethyl ether into a solution of the complex in THF.

### 3.3. Synthesis of the Hybrid Material [ $\text{MoO}_3(\text{Hpytz})$ ] (**2**)

#### 3.3.1. Reflux Hydrolysis of **1** (Method A)

Complex **1** was freshly prepared as described in Section 3.2 and immediately immersed in water (20 mL). The mixture was then heated under reflux for 17 h under nitrogen atmosphere. The resultant pale blue solid was separated from the aqueous mother liquor (pH 1–3) by filtration and washed with water ( $2 \times 10$  mL), acetone ( $2 \times 10$  mL), and diethyl ether ( $2 \times 10$  mL), and finally vacuum-dried (0.47 g, 64% based on Mo).

#### 3.3.2. Autoclave Hydrolysis of **1** (Method B)

A Teflon-lined stainless-steel autoclave was charged with **1** (0.16 g, 0.32 mmol) and water (15 mL) and heated in an oven at 100 °C for 19 h. The resultant blue solid was separated from the aqueous mother liquor by filtration and washed with water ( $2 \times 10$  mL), acetone ( $2 \times 10$  mL), and diethyl ether ( $2 \times 10$  mL), and finally vacuum-dried (0.06 g, 64% based on Mo).

#### 3.3.3. Direct Reaction of $\text{MoO}_3$ with Hpytz (Method C)

A Schlenk tube was charged with Hpytz (0.14 g, 0.95 mmol),  $\text{MoO}_3$  (0.14 g, 0.95 mmol), and water (10 mL), and heated using a conventional oil bath at 120 °C for 3 days. The mixture was allowed to cool down to room temperature and the pale blue solid was separated from the colorless solution (pH = 1–2) by filtration, washed with water ( $2 \times 10$  mL), and vacuum-dried (0.19 g, 69% based on Mo).

#### 3.3.4. Characterization Data for **2** (Method A)

Anal. Calcd. for  $\text{C}_6\text{H}_5\text{MoN}_5\text{O}_3$  (291.08): C, 24.76; H, 1.73; N, 24.06; Mo, 32.9. Found: C, 24.80; H, 1.71; N, 24.15; Mo, 32.0. FT-IR (KBr,  $\text{cm}^{-1}$ ): 3097 (w), 3059 (w), 1615 (m), 1587 (w), 1570 (w), 1547 (w), 1464 (m), 1450 (s), 1415 (w), 1388 (w), 1298 (w), 1288 (w), 1259 (w), 1226 (w), 1190 (w), 1167 (m), 1103 (w), 1089 (w), 1072 (w), 1061 (w), 1044 (w), 1022 (w), 949 (s), 917 (vs), 900 (w), 889 (vs), 833 (s), 808 (s), 768 (s), 745 (vs), 718 (s), 642 (w), 505 (w), 484 (w), 426 (w), 403 (m), 388 (m), 378 (m), 330 (s). Raman ( $\text{cm}^{-1}$ ): 3097 (w), 3060 (w), 1613 (m), 1568 (m), 1543 (m), 1011 (m), 942 (s), 916 (w), 897 (w), 887 (w), 791 (m), 720 (w).  $^{13}\text{C}\{^1\text{H}\}$  CP MAS NMR:  $\delta = 161.4$ , 158.9, 154.8, 151.1 (sh), 150.7, 148.8, 143.6, 142.7, 139.7, 129.3, 127.5, 124.3 ppm.

### 3.4. Single-Crystal X-ray Diffraction Studies

Single crystals of compound **1** were manually collected from the crystallization vial and immersed in highly viscous FOMBLIN Y perfluoropolyether vacuum oil (LVAC 140/13, Sigma-Aldrich) to prevent solvent evaporation and minimize crystal degradation [104]. Crystals were mounted on either Hampton Research CryoLoops or MiTeGen MicroLoops.

X-ray diffraction data for **1** were collected at 150(2) K on a Bruker D8 QUEST equipped with a Mo-K $\alpha$  sealed tube ( $\lambda = 0.71073$  Å), a multilayer TRIUMPH X-ray mirror, a PHOTON III CMOS detector, and an Oxford Instruments Cryostream 700+ Series cooler (Oxford Instruments, Abingdon, UK). Diffraction images were processed using SAINT+ [105], and data were corrected for absorption by the multi-scan semi-empirical method implemented in SADABS 2016/2 [106]. The structure was solved using the algorithm implemented in SHELXT-2014/5 [107], which allowed the immediate location of almost all the heaviest atoms composing the molecular unit of the compound. The remaining missing and misplaced non-hydrogen atoms were located from difference Fourier maps calculated from

successive full-matrix least-squares refinement cycles on  $F^2$  using the latest SHELXL from the 2018/3 release [108]. All structural refinements were performed using the graphical interface ShelXle [109].

Hydrogen atoms bound to carbon were placed at their idealized positions using the *HFIX 43* instruction. Hydrogen atoms associated with the N–H moieties were located from difference Fourier maps and included in the structural model with the N–H distance restrained to 0.95(1) Å. These hydrogen atoms were included in subsequent refinement cycles with isotropic thermal displacement parameters ( $U_{\text{iso}}$ ) fixed at 1.2 of the parent non-hydrogen atoms.

The last difference Fourier map synthesis showed the highest peak (0.247 eÅ<sup>-3</sup>) and the deepest hole (−0.330 eÅ<sup>-3</sup>) located at 0.74 and 1.22 Å from C4 and N7, respectively. Structural drawings were created using Crystal Impact Diamond [110].

Crystal data for **1**: C<sub>12</sub>H<sub>10</sub>Cl<sub>2</sub>MoN<sub>10</sub>O<sub>2</sub>,  $M = 493.14$ , monoclinic, space group *Ia*,  $Z = 4$ ,  $a = 7.5510(7)$  Å,  $b = 26.864(3)$  Å,  $c = 9.2340(13)$  Å,  $\beta = 105.778(3)^\circ$ ,  $V = 1802.6(3)$  Å<sup>3</sup>,  $\mu(\text{Mo-K}\alpha) = 1.057$  mm<sup>-1</sup>, colorless plate with crystal size of 0.17 × 0.10 × 0.04 mm<sup>3</sup>. From a total of 11893 reflections collected, 4003 were independent ( $R_{\text{int}} = 0.0213$ ). Final  $R1 = 0.0180$  [ $I > 2\sigma(I)$ ] and  $wR2 = 0.0414$  (all data). Data completeness to  $\theta = 25.24^\circ$ , 99.4%. CCDC 2118463.

### 3.5. Catalytic Tests

The catalytic reactions of Cy8, MeOle, MeLin, and Lim were carried out using 10 mL borosilicate reactors equipped with a Teflon valve for sampling and an appropriate Teflon-lined magnetic stirrer. Initially, catalyst **1** or **2** (in an amount equivalent to 18 μmol of Mo), organic solvent (1 mL), and substrate (1.8 mmol) were added to the reactor, which was then immersed in a temperature-controlled oil bath at 70 °C under stirring (1000 rpm). After 10 min, pre-heated TBHP (2.75 mmol for Cy8 and 3.85 mmol for the bio-based olefins) was added to the reactor, and reaction timing was counted from this instant.

Samples were taken periodically and analyzed using an Agilent 7820A GC instrument (Agilent Technologies, Santa Clara, CA, USA) equipped with a HP-5 capillary column (30 m × 0.320 mm × 0.25 μm; H<sub>2</sub> as carrier gas) and an FID detector. The quantifications of reactants/products were based on calibrations with internal standards (undecane and methyl decanoate for the substrates Cy8/Lim and MeOle/MeLin, respectively). The reaction products were identified using a Shimadzu GCMS-QP2010 Ultra equipment (Shimadzu, Kyoto, Japan) equipped with a Phenomenex capillary Zebtron ZB5-MS column (ZB-5, 30 m × 0.25 μm × 0.25 mm; He as carrier gas) and commercial databases Wiley229 (1994) and NIST14 (2014).

After the catalytic reactions with **2**, the solids were separated from the reaction mixture by centrifugation (3500 rpm); thoroughly washed with diethyl ether, ethanol, or acetone; dried overnight under atmospheric conditions; and finally vacuum-dried (ca. 0.1 bar) at 60 °C for 1 h, giving the solids denoted 2-S-run1 where S is the solvent used in the catalytic reaction. The recyclability of catalyst **2** was assessed by reusing the solids recovered after the first (2-TFT-run1) and second (2-TFT-run2) runs of the reaction Cy8/TBHP (TFT at 70 °C/24 h). The solid recovered after three catalytic runs (2-TFT-run3) was characterized by ATR FT-IR spectroscopy and PXRD. The leaching test was carried out under similar conditions to those for a normal catalytic run with TBHP/TFT at 70 °C. After 1 h, the hot reaction mixture was passed through a 0.2 μm PTFE membrane filter, and the filtrate was transferred to a separate pre-heated reactor and then stirred for a further 4 h at 70 °C. ICP-OES analysis of the liquid phase was performed to check for soluble metal species.

## 4. Conclusions

This work has demonstrated a simple hydrolysis-based method to convert a homogeneous olefin epoxidation catalyst, (H<sub>2</sub>pytz)[MoO<sub>2</sub>Cl<sub>2</sub>(pytz)] (**1**), to a heterogeneous one, [MoO<sub>3</sub>(Hpytz)] (**2**). The hybrid catalyst **2** is effective for converting biobased unsaturated fatty acid methyl esters (FAMES) and monoterpenes (Lim), giving epoxides, diols, and



(from FAMES) tetrahydrofuran-type products. Hybrid **2** may be effective for the catalytic conversion of other biomass-derived olefins to bioproducts that are useful alternatives to petrochemical-derived products.

**Supplementary Materials:** The following are available online at <https://www.mdpi.com/article/10.3390/catal11111407/s1>, CIF file for compound **1**.

**Author Contributions:** Conceptualization, A.A.V., I.S.G., and M.P.; validation, A.C.G., P.N., F.A.A.P., A.A.V., I.S.G., and M.P.; investigation, M.S.N., D.M.G., A.C.G., P.N., R.F.M., and A.D.L.; resources, F.A.A.P., A.A.V., I.S.G., and M.P.; writing—original draft preparation, M.S.N., D.M.G., A.C.G., P.N., R.F.M., and A.D.L.; writing—review and editing, F.A.A.P., A.A.V., and M.P.; visualization, M.S.N., D.M.G., A.C.G., P.N., R.F.M., A.A.V., I.S.G., and M.P.; supervision, P.N., F.A.A.P., A.A.V., I.S.G., and M.P.; project administration, P.N., A.A.V., and I.S.G.; funding acquisition, P.N. and A.A.V. All authors have read and agreed to the published version of the manuscript.

**Funding:** This work was carried out with the support of CICECO—Aveiro Institute of Materials [FCT (Fundação para a Ciência e a Tecnologia) ref. UIDB/50011/2020 & UIDP/50011/2020] and the COMPETE 2020 Operational Thematic Program for Competitiveness and Internationalization (Project POCI-01-0145-FEDER-030075), co-financed by national funds through the FCT/MCTES and the European Union through the European Regional Development Fund under the Portugal 2020 Partnership Agreement. M.S.N. (grant ref. 2021.06403.BD) and D.M.G. (grant ref. 2021.04756.BD) acknowledge the FCT for PhD grants (State Budget, European Social Fund (ESF) within the framework of PORTUGAL2020, namely through the Centro 2020 Regional Operational Programme). R.F.M. gratefully acknowledges the FCT for a Junior Research Position (CEECIND/00553/2017).

**Data Availability Statement:** Data are contained within the article or Supplementary Materials.

**Conflicts of Interest:** The authors declare no conflict of interest. The funders had no role in the design of the study; in the collection, analyses, or interpretation of data; in the writing of the manuscript; or in the decision to publish the results.

## References

1. Neochoritis, C.G.; Zhao, T.; Dömling, A. Tetrazoles via multicomponent reactions. *Chem. Rev.* **2019**, *119*, 1970–2042. [[CrossRef](#)] [[PubMed](#)]
2. Aromí, G.; Barrios, L.A.; Roubeau, O.; Gamez, P. Triazoles and tetrazoles: Prime ligands to generate remarkable coordination materials. *Coord. Chem. Rev.* **2011**, *255*, 485–546. [[CrossRef](#)]
3. Roh, J.; Vávrová, K.; Hrabálek, A. Synthesis and functionalization of 5-substituted tetrazoles. *Eur. J. Org. Chem.* **2012**, 6101–6118.
4. Mittal, R.; Awasthi, S.K. Recent Advances in the synthesis of 5-substituted 1H-tetrazoles: A complete survey (2013–2018). *Synthesis* **2019**, *51*, 3765–3783. [[CrossRef](#)]
5. Bladin, J.A. Ueber von Dicyanphenylhydrazin abgeleitete Verbindungen. *Ber. Dtsch. Chem. Ges.* **1885**, *18*, 1544–1551. [[CrossRef](#)]
6. Herr, R.J. 5-Substituted-1H-tetrazoles as carboxylic acid isosteres: Medicinal chemistry and synthetic methods. *Bioorg. Med. Chem.* **2002**, *10*, 3379–3393. [[CrossRef](#)]
7. Leyva-Ramos, S.; Cardoso-Ortiz, J. Recent developments in the synthesis of tetrazoles and their pharmacological relevance. *Curr. Org. Chem.* **2021**, *25*, 388–403. [[CrossRef](#)]
8. Dhiman, N.; Kaur, K.; Jaitak, V. Tetrazoles as anticancer agents: A review on synthetic strategies, mechanism of action and SAR studies. *Bioorg. Med. Chem.* **2020**, *28*, 115599. [[CrossRef](#)]
9. Gao, F.; Xiao, J.; Huang, G. Current scenario of tetrazole hybrids for antibacterial activity. *Eur. J. Med. Chem.* **2019**, *184*, 111744. [[CrossRef](#)]
10. Wang, T.; Gao, H.; Shreeve, J.M. Functionalized tetrazole energetics: A route to enhanced performance. *Z. Anorg. Allg. Chem.* **2021**, *647*, 157–191. [[CrossRef](#)]
11. Zhao, H.; Qu, Z.-R.; Ye, H.-Y.; Xiong, R.-G. In situ hydrothermal synthesis of tetrazole coordination polymers with interesting physical properties. *Chem. Soc. Rev.* **2008**, *37*, 84–100. [[CrossRef](#)] [[PubMed](#)]
12. Ouellette, W.; Jones, S.; Zubieta, J. Solid state coordination chemistry of metal-1,2,4-triazolates and the related metal-4-pyridyltetrazolates. *CrystEngComm* **2011**, *13*, 4457–4485. [[CrossRef](#)]
13. Rodríguez-Diéguez, A.; Mota, A.J.; Seco, J.M.; Palacios, M.A.; Romerosa, A.; Colacio, E. Influence of metal ions, coligands and reaction conditions on the structural versatility and properties of 5-pyrimidyl-tetrazolate containing complexes. *Dalton Trans.* **2009**, 9578–9586. [[CrossRef](#)] [[PubMed](#)]
14. Yang, E.-C.; Feng, Y.; Liu, Z.-Y.; Liu, T.-Y.; Zhao, X.-J. Diverse mixed-ligand metal complexes with in situ generated 5-(pyrazinyl) tetrazolate chelating-bridging ligand: In situ synthesis, crystal structures, magnetic and luminescent properties. *CrystEngComm* **2011**, *13*, 230–242. [[CrossRef](#)]

15. Gaponik, P.N.; Voitekhovich, S.V.; Ivashkevich, O.A. Metal derivatives of tetrazoles. *Russ. Chem. Rev.* **2006**, *75*, 507–539. [[CrossRef](#)]
16. Liu, M.-g.; Zhang, P.-p.; Peng, J.; Meng, H.-x.; Wang, X.; Zhu, M.; Wang, D.-d.; Meng, C.-l.; Alimaje, K. Organic–inorganic hybrids constructed from mixed-valence multinuclear copper complexes and templated by Keggin polyoxometalates. *Cryst. Growth Des.* **2012**, *12*, 1273–1281. [[CrossRef](#)]
17. Wu, X.-Y.; Zhang, Q.-K.; Kuang, X.-F.; Yang, W.-B.; Yu, R.-M.; Lu, C.-Z. Two hybrid polyoxometalate-pillared metal–organic frameworks. *Dalton Trans.* **2012**, *41*, 11783–11787. [[CrossRef](#)] [[PubMed](#)]
18. Darling, K.; Ouellette, W.; Prosvirin, A.; Freund, S.; Dunbar, K.R.; Zubieta, J. Solid state coordination chemistry of the copper(II)/pyridyl- and pyrazine-tetrazolate/sulfate system. *Cryst. Growth Des.* **2012**, *12*, 2662–2672. [[CrossRef](#)]
19. Lin, P.; Clegg, W.; Harrington, R.W.; Henderson, R.A. Synthesis and structures of 5-(pyridyl) tetrazole complexes of Mn(II). *Dalton Trans.* **2005**, 2388–2394. [[CrossRef](#)]
20. Dong, P.; Zhang, Q.-K.; Wang, F.; Chen, S.-C.; Wu, X.-Y.; Zhao, Z.-G.; Lu, C.-Z. A new molybdenum-oxide-based organic-inorganic hybrid compound templated by 5-(2-pyridyl) tetrazole with new topology and canted antiferromagnetism. *Cryst. Growth Des.* **2010**, *10*, 3218–3221. [[CrossRef](#)]
21. Mo, X.-J.; Gao, E.-Q.; He, Z.; Li, W.-J.; Yan, C.-H. An unexpected in situ formation of a substitute tetrazole ligand and its Mn (II) and Cu(II) complexes. *Inorg. Chem. Commun.* **2004**, *7*, 353–355. [[CrossRef](#)]
22. Fiorini, V.; Ranieri, A.M.; Muzzioli, S.; Magee, K.D.M.; Zacchini, S.; Akabar, N.; Stefan, A.; Ogden, M.I.; Massi, M.; Stagni, S. Targeting divalent metal cations with Re(I) tetrazolato complexes. *Dalton Trans.* **2015**, *44*, 20597–20608. [[CrossRef](#)] [[PubMed](#)]
23. Hu, M.; Ma, S.-T.; Guo, L.-Q.; Fang, S.-M. Diaquabis [5-(2-pyridyl) tetrazolato- $K^2N^1, N^5$ ] iron(II). *Acta Crystallogr. Sect. E Struct. Rep. Online* **2009**, *65*, m382. [[CrossRef](#)] [[PubMed](#)]
24. Ghosh, K.; Banerjee, A.; Bauzá, A.; Frontera, A.; Chattopadhyay, S. One pot synthesis of two cobalt(III) schiff base complexes with chelating pyridyltetrazolate and exploration of their bio-relevant catalytic activities. *RSC Adv.* **2018**, *8*, 28216–28237. [[CrossRef](#)]
25. Nasani, R.; Saha, M.; Mobin, S.M.; Mukhopadhyay, S. Microwave synthesis of mono- and bis-tetrazolato complexes via 1,3-dipolar cycloaddition of organonitriles with nickel(II)-bound azides: Isolation of 5-substituted tetrazoles from parent complex. *Polyhedron* **2013**, *55*, 24–36. [[CrossRef](#)]
26. Das, M.; Chatterjee, S.; Harms, K.; Mondal, T.K.; Chattopadhyay, S. Formation of bis ( $\mu$ -tetrazolato) dinickel(II) complexes with N,N,O-donor Schiff bases via in situ 1,3-dipolar cyclo-additions: Isolation of a novel bi-cyclic trinuclear nickel(II)–sodium(I)–nickel(II) complex. *Dalton Trans.* **2014**, 2936–2947. [[CrossRef](#)] [[PubMed](#)]
27. Mukhopadhyay, B.G.; Mukhopadhyay, S.; Guedes da Silva, M.F.C.; Charmier, M.A.J.; Pombeiro, A.J.L. Synthesis of mono- and bis-tetrazolato Complexes of Ni(II), Pt(II) and Cu(II) via 1,3-dipolar cycloadditions of 2-cyanopyridines with metal ligated azides in N,N,O-aminoiminophenolato complexes. *Dalton Trans.* **2009**, 4778–4785. [[CrossRef](#)] [[PubMed](#)]
28. Cui, J.; Zhao, H.; Zhao, J. Unprecedented preparation of a unique 2D multinuclear copper metal-tetrazole polymer by in situ solvothermal reaction: Crystal structure and magnetic property. *Inorg. Chem. Commun.* **2013**, *31*, 1–4. [[CrossRef](#)]
29. Wang, L.-Z.; Qu, Z.-R.; Zhao, H.; Wang, X.-S.; Xiong, R.-G.; Xue, Z.-L. Isolation and crystallographic characterization of a solid precipitate/intermediate in the preparation of 5-substituted 1H-tetrazoles from nitrile in water. *Inorg. Chem.* **2003**, *42*, 3969–3971. [[CrossRef](#)] [[PubMed](#)]
30. Zhang, L. Bis [ $\mu$ -5-(2-pyridyl) tetrazolato]- $K^3N^1, N^5:N^2; K^3N^2:N^1, N^5$ -bis [triaquazinc(II)] bis (trifluoroacetate) monohydrate. *Acta Crystallogr. Sect. E Struct. Rep. Online* **2009**, *65*, m871–m872. [[CrossRef](#)] [[PubMed](#)]
31. Yu, X.-Y.; Zhang, R.; Li, S.-L.; Yu, S.-H.; Gao, L.; Yan, W.-F.; Jin, J.; Luo, Y.-N. A new silver-organic coordination polymer: Synthesis, crystal structure, fluorescence and antibacterial activity. *Inorg. Chem. Commun.* **2020**, *116*, 107897. [[CrossRef](#)]
32. Darling, K.; Ouellette, W.; Pellizzeri, S.; Smith, T.; Vargas, J.; Tomaszfski, S.; O'Connor, C.J.; Zubieta, J. One- and two-dimensional coordination polymers of substituted tetrazoles with cadmium(II). *Inorg. Chim. Acta* **2012**, *392*, 417–427. [[CrossRef](#)]
33. Bhaumik, P.K.; Roy, S.; Harms, K.; Chattopadhyay, S. Formation of novel cadmium(II) tetrazolato complexes with Schiff bases as co-ligands via in situ [3+2] cyclo-addition. *Polyhedron* **2014**, *81*, 168–179. [[CrossRef](#)]
34. Mrowiec, A.; Jurowska, A.; Hodorowicz, M.; Szklarzewicz, J. 5-(2-pyridyl)-1H-tetrazole complexes with Mo(IV) and W(IV) cyanides. *Dalton Trans.* **2017**, *46*, 4030–4037. [[CrossRef](#)] [[PubMed](#)]
35. Yang, M.-X.; Chen, L.-J.; Lin, S.; Chen, X.-H.; Huang, H. Inorganic–organic hybrid compounds based on molybdenum oxide chains and tetrazolate-bridged polymeric silver cations. *Dalton Trans.* **2011**, *40*, 1866–1872. [[CrossRef](#)]
36. Wu, X.-Y.; Dong, P.; Yu, R.; Zhang, Q.-K.; Kuang, X.; Chen, S.-C.; Lin, Q.-P.; Lu, C.-Z. A 2D polyoxometalate-based complex: Spin-canting and metamagnetism. *CrystEngComm* **2011**, *13*, 3686–3688. [[CrossRef](#)]
37. Wang, X.; Li, T.; Tian, A.; Zhang, R. The rigid isomeric 5-(x-pyridyl)-1H-tetrazole ligands-directed various isopolymolybdate-based compounds: Assembly, structures, and properties. *J. Coord. Chem.* **2016**, *69*, 1–11. [[CrossRef](#)]
38. Wang, X.-L.; Li, T.-J.; Tian, A.-X.; Li, N.; Yang, Y.; Ning, Y.-L.; Hou, X. Influence of N-donor sites in 5-(x-pyridyl)-1H-tetrazole ligands ( $x = 2, 4$ ) on assembly of polyoxometalate-based compounds modified by multinuclear metal clusters and infinite chains. *CrystEngComm* **2015**, *17*, 3257–3267. [[CrossRef](#)]
39. Xue, C.-M.; Li, S.-X.; Zhang, L.; Sha, J.-Q.; Zheng, T.-Y.; Zhang, Q.-N.; Li, L. Hydrothermal synthesis, characterization and electrocatalytic/photocatalytic activities of new polyoxometalate based hybrid compound. *J. Inorg. Organomet. Polym.* **2013**, *23*, 1468–1476. [[CrossRef](#)]

40. Neves, P.; Amarante, T.R.; Gomes, A.C.; Coelho, A.C.; Gago, S.; Pillinger, M.; Gonçalves, I.S.; Silva, C.M.; Valente, A.A. Heterogeneous oxidation catalysts formed in situ from molybdenum tetracarbonyl complexes and *tert*-butyl hydroperoxide. *Appl. Catal. A: Gen.* **2011**, *395*, 71–77. [[CrossRef](#)]
41. Amarante, T.R.; Neves, P.; Gomes, A.C.; Nolasco, M.; Ribeiro-Claro, P.; Coelho, A.C.; Valente, A.A.; Paz, F.A.A.; Smeets, S.; McCusker, L.B.; et al. Synthesis, structural elucidation, and catalytic properties in olefin epoxidation of the polymeric hybrid material  $[\text{Mo}_3\text{O}_9(2\text{-}[3(5)\text{-pyrazolyl}]\text{pyridine})]_n$ . *Inorg. Chem.* **2014**, *53*, 2652–2665. [[CrossRef](#)] [[PubMed](#)]
42. Coelho, A.C.; Nolasco, M.; Balula, S.S.; Antunes, M.M.; Pereira, C.C.L.; Paz, F.A.A.; Valente, A.A.; Pillinger, M.; Ribeiro-Claro, P.; Klinowski, J.; et al. Chemistry and catalytic activity of molybdenum(VI)-pyrazolylpyridine complexes in olefin epoxidation. Crystal structures of monomeric dioxo, dioxo- $\mu$ -oxo, and oxodiperoxo derivatives. *Inorg. Chem.* **2011**, *50*, 525–538. [[CrossRef](#)] [[PubMed](#)]
43. Li, D.; Liu, Y.; Wei, P.; Hu, B.; Zhang, X. Tetra- $\mu$ -oxido-tetrakis {dioxide [3-(2-pyridyl)-1H-pyrazole] molybdenum(VI)}. *Acta Crystallogr. Sect. E Struct. Rep. Online* **2009**, *65*, m1074.
44. Groom, C.R.; Bruno, I.J.; Lightfoot, M.P.; Ward, S.C. The Cambridge Structural Database. *Acta Crystallogr. Sect. B Struct. Sci. Cryst. Eng. Mater.* **2016**, *72*, 171–179. [[CrossRef](#)]
45. Klein, A.; Krest, A.; Nitsche, S.; Stirnat, K.; Valldor, M. First homoleptic complexes of the tridentate pyridine-2,6-ditrazolate ligand. *Eur. J. Inorg. Chem.* **2013**, 2757–2767. [[CrossRef](#)]
46. Mosalkova, A.P.; Voitekhovich, S.V.; Lyakhov, A.S.; Ivashkevich, L.S.; Gaponik, P.N.; Ivashkevich, O.A. Direct synthesis and characterization of new copper(II) and zinc(II) 5-*R*-tetrazolato complexes [*R* = Me, Ph, 4-Py] with ethylenediamine and DMSO as coligands. *Z. Anorg. Allg. Chem.* **2012**, *638*, 103–110. [[CrossRef](#)]
47. Nunes, M.S.; Neves, P.; Gomes, A.C.; Cunha-Silva, L.; Valente, A.A.; Pillinger, M.; Gonçalves, I.S. A Silicododecamolybdate/pyridinium-tetrazole hybrid molecular salt as a catalyst for the epoxidation of bio-derived olefins. *Inorg. Chim. Acta* **2021**, *516*, 120129. [[CrossRef](#)]
48. Paciorek, P.; Szklarzewicz, J.; Nitek, W. A simple and safe method for the preparation of bis [2-(2H-tetrazol-5-yl)-pyridinium] tetrachloridozincate(II). *Acta Crystallogr. Sect. C Cryst. Struct. Commun.* **2013**, *69*, 513–516. [[CrossRef](#)]
49. Demko, Z.P.; Sharpless, K.B. Preparation of 5-substituted 1H-tetrazoles from nitriles in water. *J. Org. Chem.* **2001**, *66*, 7945–7950. [[CrossRef](#)]
50. Andrews, P.C.; Beck, T.; Fraser, B.H.; Junk, P.C.; Massi, M. Synthesis and structural characterisation of cationic, neutral and hydroxo-bridged lanthanoid (La, Gd, Ho, Yb, Y) bis 5-(2-pyridyl)tetrazolate complexes. *Polyhedron* **2007**, *26*, 5406–5413. [[CrossRef](#)]
51. Stagni, S.; Orselli, E.; Palazzi, A.; Cola, L.D.; Zacchini, S.; Femoni, C.; Marcaccio, M.; Paolucci, F.; Zanarini, S. Polypyridyl ruthenium(II) complexes with tetrazolate-based chelating ligands. Synthesis, reactivity, and electrochemical and photophysical properties. *Inorg. Chem.* **2007**, *46*, 9126–9138. [[CrossRef](#)]
52. Guan, Y.; Sowndarya, S.V.S.; Gallegos, L.C.; St. John, P.C.; Paton, R.S. Real-time prediction of  $^1\text{H}$  and  $^{13}\text{C}$  chemical shifts with DFT accuracy using a 3D graph neural network. *Chem. Sci.* **2021**, *12*, 12012–12026. [[CrossRef](#)] [[PubMed](#)]
53. Andrews, P.C.; Junk, P.C.; Massi, M.; Silberstein, M. Gelation of La(III) cations promoted by 5-(2-pyridyl) tetrazolate and water. *Chem. Commun.* **2006**, 3317–3319. [[CrossRef](#)]
54. Abrantes, M.; Amarante, T.R.; Antunes, M.M.; Gago, S.; Paz, F.A.A.; Margiolaki, I.; Rodrigues, A.E.; Pillinger, M.; Valente, A.A.; Gonçalves, I.S. Synthesis, structure, and catalytic performance in cyclooctene epoxidation of a molybdenum oxide/bipyridine hybrid material:  $[\text{MoO}_3(\text{bipy})][\text{MoO}_3(\text{H}_2\text{O})]_n$ . *Inorg. Chem.* **2010**, *49*, 6865–6873. [[CrossRef](#)] [[PubMed](#)]
55. Amarante, T.R.; Neves, P.; Tomé, C.; Abrantes, M.; Valente, A.A.; Paz, F.A.A.; Pillinger, M.; Gonçalves, I.S. An octanuclear molybdenum(VI) complex containing coordinatively bound 4,4'-di-*tert*-butyl-2,2'-bipyridine,  $[\text{Mo}_8\text{O}_{22}(\text{OH})_4(\text{di-}t\text{-Bu-bipy})_4]$ : Synthesis, structure, and catalytic epoxidation of bio-derived olefins. *Inorg. Chem.* **2012**, *51*, 3666–3676. [[CrossRef](#)]
56. Figueiredo, S.; Gomes, A.C.; Neves, P.; Amarante, T.R.; Paz, F.A.A.; Soares, R.; Lopes, A.D.; Valente, A.A.; Pillinger, M.; Gonçalves, I.S. Synthesis, structural elucidation, and application of a pyrazolylpyridine–molybdenum oxide composite as a heterogeneous catalyst for olefin epoxidation. *Inorg. Chem.* **2012**, *51*, 8629–8635. [[CrossRef](#)] [[PubMed](#)]
57. Amarante, T.R.; Neves, P.; Paz, F.A.A.; Valente, A.A.; Pillinger, M.; Gonçalves, I.S. Investigation of a dichlorodioxomolybdenum(VI)-pyrazolylpyridine complex and a hybrid derivative as catalysts in olefin epoxidation. *Dalton Trans.* **2014**, *43*, 6059–6069. [[CrossRef](#)]
58. Neves, P.; Nogueira, L.S.; Gomes, A.C.; Oliveira, T.S.M.; Lopes, A.D.; Valente, A.A.; Gonçalves, I.S.; Pillinger, M. Chemistry and catalytic performance of pyridyl-benzimidazole oxidomolybdenum(VI) compounds in (bio)olefin epoxidation. *Eur. J. Inorg. Chem.* **2017**, 2617–2627. [[CrossRef](#)]
59. Wright, P.J.; Muzzioli, S.; Skelton, B.W.; Raiteri, P.; Lee, J.; Koutsantonis, G.; Silvester, D.S.; Stagni, S.; Massi, M. One-step assembly of Re(I) tricarbonyl 2-pyridyltetrazolato metallacalix[3]arene with aqua emission and reversible three-electron oxidation. *Dalton Trans.* **2013**, *42*, 8188–8191. [[CrossRef](#)]
60. Morlot, J.; Uytbroeck, N.; Agustin, D.; Poli, R. Solvent-free epoxidation of olefins catalyzed by “[ $\text{MoO}_2(\text{SAP})$ ]”: A new mode of *tert*-butylhydroperoxide activation. *ChemCatChem* **2013**, *5*, 601–611. [[CrossRef](#)]
61. Comas-Vives, A.; Lledós, A.; Poli, R. A Computational study of the olefin epoxidation mechanism catalyzed by cyclopentadienyl-oxidomolybdenum(VI) complexes. *Chem. Eur. J.* **2010**, *16*, 2147–2158. [[CrossRef](#)] [[PubMed](#)]
62. Thiel, W.R.; Priermeier, T. The first olefin-substituted peroxomolybdenum complex: Insight into a new mechanism for the Molybdenum-catalyzed epoxidation of olefins. *Angew. Chem. Int. Ed. Engl.* **1995**, *34*, 1737–1738. [[CrossRef](#)]
63. Thiel, W.R.; Eppinger, J. Molybdenum-catalyzed olefin epoxidation: Ligand effects. *Chem. Eur. J.* **1997**, *3*, 696–705. [[CrossRef](#)]



64. Calhorda, M.J.; Costa, P.J. Unveiling the mechanisms of catalytic oxidation reactions mediated by oxo-molybdenum complexes: A computational overview. *Curr. Org. Chem.* **2012**, *16*, 65–72. [CrossRef]
65. Veiros, L.F.; Prazeres, A.; Costa, P.J.; Romão, C.C.; Kühn, F.E.; Calhorda, M.J. Olefin epoxidation with *tert*-butyl hydroperoxide catalyzed by MoO<sub>2</sub>X<sub>2</sub>L complexes: A DFT mechanistic study. *Dalton Trans.* **2006**, 1383–1389. [CrossRef] [PubMed]
66. Costa, P.J.; Calhorda, M.J.; Kühn, F.E. Olefin epoxidation catalyzed by η<sup>5</sup>-cyclopentadienyl molybdenum compounds: A computational study. *Organometallics* **2010**, *29*, 303–311. [CrossRef]
67. Kühn, F.E.; Groarke, M.; Bencze, É.; Herdtweck, E.; Prazeres, A.; Santos, A.M.; Calhorda, M.J.; Romão, C.C.; Gonçalves, I.S.; Lopes, A.D.; et al. Octahedral bipyridine and bipyrimidine dioxomolybdenum(VI) complexes: Characterization, application in catalytic epoxidation, and density functional mechanistic study. *Chem. Eur. J.* **2002**, *8*, 2370–2383. [CrossRef]
68. Chniti, S.; Hassouna, M. Ethanol fuel from biomass: A review. *Eur. J. Chem. Environ. Eng. Sci.* **2017**, *1*, 1–7.
69. Dielectric Constant. Available online: <https://www.flowline.com/dielectric-constant> (accessed on 5 July 2021).
70. Lysenko, A.B.; Senchyk, G.A.; Domasevitch, K.V.; Hauser, J.; Fuhrmann, D.; Kobalz, M.; Krautscheid, H.; Neves, P.; Valente, A.A.; Gonçalves, I.S. Synthesis and structural elucidation of triazolylmolybdenum(VI) oxide hybrids and their behavior as oxidation catalysts. *Inorg. Chem.* **2015**, *54*, 8327–8338. [CrossRef] [PubMed]
71. Amarante, T.R.; Neves, P.; Paz, F.A.A.; Gomes, A.C.; Pillinger, M.; Valente, A.A.; Gonçalves, I.S. Heterogeneous catalysis with an organic-inorganic hybrid based on MoO<sub>3</sub> chains decorated with 2,2'-biimidazole ligands. *Catal. Sci. Technol.* **2021**, *11*, 2214–2228. [CrossRef]
72. Asgharpour, Z.; Farzaneh, F.; Abbasi, A.; Ghiasi, M. Synthesis, crystal structure and DFT studies of a new dioxomolybdenum(VI) Schiff base complex as an olefin epoxidation catalyst. *Polyhedron* **2015**, *101*, 282–289. [CrossRef]
73. Rayati, S.; Abdolalian, P. Sonochemical syntheses of nano-sized dioxomolybdenum complexes: An efficient, selective and reusable heterogeneous nanocatalyst for oxidation of alkenes. *Appl. Catal. A Gen.* **2013**, *456*, 240–248. [CrossRef]
74. Bagherzadeh, M.; Zare, M. Synthesis, characterization, and catalysis of recyclable new piperazine-bridged Mo(VI) polymers [MoO<sub>2</sub> (Salen) (piperazine)]<sub>n</sub> in highly selective oxygenation of alkenes and sulfides. *J. Coord. Chem.* **2013**, *66*, 2885–2900. [CrossRef]
75. Du, J.; Yu, J.; Tang, J.; Wang, J.; Zhang, W.; Thiel, W.R.; Jia, M. Supramolecular assemblies directed by hydrogen bonds and π–π interactions and based on *N*-heterocyclic-ligand-modified β-octamolybdate—Structure and catalytic application in olefin epoxidation. *Eur. J. Inorg. Chem.* **2011**, 2361–2365. [CrossRef]
76. Abdalghani, I.; Biancalana, L.; Aschi, M.; Pampaloni, G.; Marchetti, F.; Crucianelli, M. Dioxomolybdenum(VI) compounds with α-amino acid donor ligands as catalytic precursors for the selective oxyfunctionalization of olefins. *Mol. Catal.* **2018**, *446*, 39–48. [CrossRef]
77. Hosseinyzade, S.S.; Zonoz, F.M.; Bahramian, B. Synthesis, characterization, and application of a new nanohybrid Schiff base polyoxometalate in epoxidation of olefins in the presence of *tert*-butyl hydroperoxide. *J. Coord. Chem.* **2020**, *73*, 243–254. [CrossRef]
78. Armylisas, A.H.N.; Hazirah, M.F.S.; Yeong, S.K.; Hazimah, A.H. Modification of olefinic double bonds of unsaturated fatty acids and other vegetable oil derivatives via epoxidation: A review. *Grasas Y Aceites* **2017**, *68*, e174. [CrossRef]
79. Corma, A.; Iborra, S.; Velty, A. Chemical routes for the transformation of biomass into chemicals. *Chem. Rev.* **2007**, *107*, 2411–2502. [CrossRef] [PubMed]
80. Carvalho, M.S.; Mendonça, M.A.; Pinho, D.M.M.; Resck, I.S.; Suarez, P.A.Z. Chromatographic analyses of fatty acid methyl esters by HPLC-UV and GC-FID. *J. Braz. Chem. Soc.* **2012**, *23*, 763–769. [CrossRef]
81. Nameer, S.; Deltin, T.; Sundell, P.-E.; Johansson, M. Bio-based multifunctional fatty acid methyl esters as reactive diluents in coil coatings. *Prog. Org. Coatings* **2019**, *136*, 105277. [CrossRef]
82. Lv, N.; He, W.; Fang, Z.; Sun, Q.; Qiu, C.; Guo, K. Epoxidation of methyl oleate and subsequent ring-opening catalyzed by lipase from *Candida* sp. 99–125. *Eur. J. Lipid Sci. Technol.* **2018**, *120*, 1700257. [CrossRef]
83. Wang, J.; Zhao, X.; Liu, D. Preparation of epoxidized fatty acid methyl ester with in situ auto-catalyzed generation of performic acid and the influence of impurities on epoxidation. *Waste Biomass Valor.* **2018**, *9*, 1881–1891. [CrossRef]
84. Doll, K.M.; Erhan, S.Z. Synthesis and performance of surfactants based on epoxidized methyl oleate and glycerol. *J. Surfact. Deterg.* **2006**, *9*, 377–383. [CrossRef]
85. Tang, J.; Zhang, J.; Lu, J.; Huang, J.; Zhang, F.; Hu, Y.; Liu, C.; An, R.; Miao, H.; Chen, Y.; et al. Preparation and properties of plant-oil-based epoxy acrylate-like resins for UV-curable coatings. *Polymers* **2012**, *12*, 2165. [CrossRef] [PubMed]
86. Borugadda, V.B.; Goud, V.V. Epoxidation of castor oil fatty acid methyl esters (COFAME) as a lubricant base stock using heterogeneous ion-exchange resin (IR-120) as a catalyst. *Energy Procedia* **2014**, *54*, 75–84. [CrossRef]
87. Hölderich, W.F.; Rios, L.A.; Weckes, P.P. Investigations into the epoxidation and alcoholysis of oleochemicals for use as lubricants. *J. Synth. Lubr.* **2004**, *20*, 289–301. [CrossRef]
88. Lligadas, G.; Ronda, J.C.; Galià, M.; Biermann, U.; Metzger, J.O. Synthesis and characterization of polyurethanes from epoxidized methyl oleate based polyether polyols as renewable resources. *J. Polym. Sci. Part A Polym. Chem.* **2006**, *44*, 634–645. [CrossRef]
89. Miao, S.; Wang, P.; Su, Z.; Zhang, S. Vegetable-oil-based polymers as future polymeric biomaterials. *Acta Biomater.* **2014**, *10*, 1692–1704. [CrossRef] [PubMed]
90. He, W.; Zhu, G.; Gao, Y.; Wu, H.; Fang, Z.; Guo, K. Green plasticizers derived from epoxidized soybean oil for poly (vinyl chloride): Continuous synthesis and evaluation in PVC films. *Chem. Eng. J.* **2020**, *380*, 122532. [CrossRef]

91. Debal, A.; Rafaralahitsimba, G.; Bonfan, A.; Ucciani, E. Catalytic epoxidation of methyl linoleate—cyclisation products of the epoxyacid esters. *Fat Sci. Technol.* **1995**, *97*, 269–273. [[CrossRef](#)]
92. Borhan, B.; Nourooz-Zadeh, J.; Uematsu, T.; Hammock, B.D.; Kurth, M.J. Stereochemical aspects of cytosolic epoxide hydrolase hydration of methyl diepoxystearates. *Tetrahedron* **1993**, *49*, 2601–2612. [[CrossRef](#)]
93. Piazza, G.J.; Nuñez, A.; Foglia, T.A. Hydrolysis of mono- and diepoxyoctadecanoates by alumina. *J. Am. Oil Chem. Soc.* **2003**, *80*, 901–904. [[CrossRef](#)]
94. Bantchev, G.B.; Doll, K.M.; Biresaw, G.; Vermillion, K.E. Formation of furan fatty alkyl esters from their bis-epoxide fatty esters. *J. Am. Oil Chem. Soc.* **2014**, *91*, 2117–2123. [[CrossRef](#)]
95. Costa, V.V.; da Silva Rocha, K.A.; Kozhevnikov, I.V.; Kozhevnikova, E.F.; Gusevskaya, E.V. Heteropoly acid catalysts for the synthesis of fragrance compounds from biorenewables: Isomerization of limonene oxide. *Catal. Sci. Technol.* **2013**, *3*, 244–250. [[CrossRef](#)]
96. Nguyen, T.-T.T.; Chau, D.-K.N.; Duus, F.; Le, T.N. Green synthesis of carvenone by montmorillonite-catalyzed isomerization of 1,2-limonene oxide. *Int. J. Org. Chem.* **2013**, *3*, 206–209. [[CrossRef](#)]
97. Ferrarini, S.R.; Graebin, C.S.; Limberger, J.; Canto, R.F.S.; Dias, D.O.; da Rosa, R.G.; Madeira, M.D.F.; Eifler-lima, V.L. Synthesis of limonene  $\beta$ -amino alcohol derivatives in support of new antileishmanial therapies. *Mem. Inst. Oswaldo Cruz* **2008**, *103*, 773–777. [[CrossRef](#)] [[PubMed](#)]
98. Li, C.; Veldhuis, T.; Reuvers, B.; Sablong, R.J.; Koning, C.E. Fully renewable limonene-derived polycarbonate as a high-performance alkyd resin. *Polym. Int.* **2020**, *69*, 24–30. [[CrossRef](#)]
99. Ciriminna, R.; Lomeli-Rodrigues, M.; Lopez-Sanchez, J.A.; Pagliaro, M. Limonene: A versatile chemical of the bioeconomy. *Chem. Commun.* **2014**, *50*, 15288–15296. [[CrossRef](#)] [[PubMed](#)]
100. Dipentene Dioxide. Available online: <http://chemicaland21.com/specialtychem/nh/DIPENTENE%20DIOXIDE.htm> (accessed on 29 October 2021).
101. Li, C.; Sablong, R.J.; Koning, C.E. Chemoselective alternating copolymerization of limonene dioxide and carbon Dioxide: A new highly functional aliphatic epoxy polycarbonate. *Angew. Chem. Int. Ed.* **2016**, *55*, 11572–11576. [[CrossRef](#)]
102. Schutz, L.; Kazemi, F.; Mackenzie, E.; Bergeron, J.-Y.; Gagnon, E.; Claverie, J.P. *Trans*-limonene dioxide, a promising bio-based epoxy monomer. *J. Polym. Sci.* **2021**, *59*, 321–328. [[CrossRef](#)]
103. Bähr, M.; Bitto, A.; Mülhaupt, R. Cyclic limonene dicarbonate as a new monomer for non-isocyanate oligo- and polyurethanes (NIPU) based upon terpenes. *Green Chem.* **2012**, *14*, 1447–1454. [[CrossRef](#)]
104. Kottke, T.; Stalke, D. Crystal handling at low temperatures. *J. Appl. Crystallogr.* **1993**, *26*, 615–619. [[CrossRef](#)]
105. SAINT+. *Data Integration Engine v. 8.37a*©; Bruker AXS: Madison, WI, USA, 2015.
106. Krause, L.; Herbst-Irmer, R.; Sheldrick, G.M.; Stalke, D. Comparison of silver and molybdenum microfocus X-ray sources for single-crystal structure determination. *J. Appl. Crystallogr.* **2015**, *48*, 3–10. [[CrossRef](#)] [[PubMed](#)]
107. Sheldrick, G.M. SHELXT—Integrated space-group and crystal-structure determination. *Acta Crystallogr. Sect. A Found. Adv.* **2015**, *71*, 3–8. [[CrossRef](#)]
108. Sheldrick, G.M. Crystal structure refinement with SHELXL. *Acta Crystallogr. Sect. C Struct. Chem.* **2015**, *71*, 3–8. [[CrossRef](#)]
109. Hübschle, C.B.; Sheldrick, G.M.; Dittrich, B. ShelXle: A Qt graphical user interface for SHELXL. *J. Appl. Crystallogr.* **2011**, *44*, 1281–1284. [[CrossRef](#)]
110. Brandenburg, K. *Diamond, Version 3.2f*; Crystal Impact GbR: Bonn, Germany, 2010.